Title: Biosurfactant production maintains viability in anoxic conditions by depolarizing the membrane in *Bacillus subtilis*

Authors

Heidi A. Arjes[1], Lam Vo[1], Caroline Marie Dunn[2], Lisa Willis[1], Christopher A. DeRosa[3], Cassandra L. Fraser[3], Daniel B. Kearns[2,*], Kerwyn Casey Huang[1,4,5,*]

Affiliations

[1]Department of Bioengineering, Stanford University School of Medicine, Stanford, CA 94305, USA

[2]Department of Biology, Indiana University, Bloomington, IN 47405, USA

[3]Department of Chemistry, University of Virginia, Charlottesville, VA 22904, USA

[4]Department of Microbiology & Immunology, Stanford University School of Medicine, Stanford, CA 94305, USA

[5]Chan Zuckerberg Biohub, San Francisco, CA 94158

*Corresponding authors: kchuang@stanford.edu and dbkearns@indiana.edu

Lead author: Kerwyn Casey Huang (kchuang@stanford.edu)

Keywords: surfactin, biosurfactant, oxygen depletion, cell lysis, protoplast, respiration, membrane potential, membrane energetics, LytC

Summary

The presence or absence of oxygen in the environment is a strong effector of cellular metabolism and physiology. Like many eukaryotes and some bacteria, *Bacillus subtilis* is an obligate aerobe that primarily utilizes oxygen during respiration to generate ATP. Despite the importance of oxygen for *B. subtilis* survival, we know little about how oxygen is consumed during growth and how populations respond to shifts in oxygen availability. Here, we find that when oxygen was depleted from stationary phase cultures ~90% of *B. subtilis* 3610 cells died and lysed due to autolysin activity; the remaining cells maintained colony-forming ability. Interestingly, the domesticated 168 strain maintained a higher optical density than 3610 during oxygen depletion due to the formation of cell-wall-less protoplasts, but the remaining, rod-shaped cells were >100-fold less viable than 3610. We discovered that the higher viability in 3610 was due to its ability to produce the antibacterial compound surfactin, as surfactin addition rescued 168 viability and also increased yield in aerobic growth. We further demonstrate that surfactin strongly depolarizes the *B. subtilis* membrane, and that other known membrane-potential disruptors restore viability to 168. These findings highlight the importance of surfactin for survival during oxygen-depleted conditions and demonstrate that antimicrobials normally considered harmful can instead benefit cells in stressful conditions when the terminal electron acceptor in respiration is limiting.

41 **Introduction**

42

43 Many species across all domains of life use oxygen as the terminal electron acceptor during
44 aerobic respiration, which produces approximately ten-fold more ATP per glucose
45 molecule than via glycolysis and fermentation in the absence of respiration. In most human
46 cells, oxygen depletion causes exhaustion of ATP and eventual death, either through lysis
47 caused by osmotic stress due to the inability to regulate osmolyte levels [1, 2] or through
48 activation of signaling cascades that lead to apoptosis [3]. Thus, maintaining concentration
49 gradients of ions across cell membranes is of paramount importance when oxygen is
50 lacking. Like human cells, certain microbes such as the pathogen *Mycobacterium*
51 *tuberculosis* as well as most fungi (with the exception of yeasts) [4] are considered strict
52 aerobes due to their inability to make ATP in the absence of oxygen. Under conditions of
53 rapidly depleted oxygen, *M. tuberculosis* cells show a loss in viability [5, 6]. The related,
54 soil-dwelling species *Mycobacterium smegmatis* also loses viability upon oxygen depletion,
55 and the remaining viable cells maintain the redox balance using hydrogen fermentation
56 and activate stress response genes critical for survival [7, 8]. Despite the clinical
57 importance of *M. tuberculosis*, surprisingly few studies have interrogated how these and
58 other strict aerobes respond to oxygen depletion and the genes responsible for survival.
59 The Gram-positive model bacterium *Bacillus subtilis* is considered a strict aerobe
60 when grown in the absence of nitrate or nitrite [9]. *B. subtilis* is naturally found in the soil
61 and is used as an additive to help prevent infections and promote growth in plants [10, 11].
62 In the soil, *B. subtilis* undergoes constant shifts in oxygen concentration, as oxygen is
63 readily available in dry soils but diffuses less and becomes depleted in wet or flooded soils

64 following a rain [12]. Early observations of *B. subtilis* culture lysis upon a shift to anoxic
65 environments have yet to be further characterized [13], and it remains a mystery whether
66 *B. subtilis* has strategies to cope with oxygen limitation.

67 *B. subtilis* has long been domesticated in the lab, leading to a multitude of genetic
68 tools, strain libraries, and online databases and resources [14-16]. The high level of genetic
69 relatedness between biofilm-forming "wild" strains and derivative non-biofilm-forming
70 laboratory strains has been exploited to identify genetic differences that underlie biofilm
71 community behaviors [17]. For instance, the commonly studied laboratory strain 168,
72 which is derived from the biofilm-forming strain 3610, lacks an extrachromosomal plasmid
73 and harbors several point mutations that reduce or abolish social behaviors such as matrix
74 production [18]. Notably, 3610 produces the small molecule surfactin, a powerful
75 surfactant that has previously been implicated in swarming motility [19-21]. Surfactin has
76 also been shown to kill fungi [22] and some bacteria *in vitro* [22-26]. However, fitness
77 benefits of surfactin production in the context of planktonic cultures have yet to be
78 identified, although some surfactants can accelerate oxygen diffusion through the air-water
79 interface [27].

80 Here, we characterize the interplay between oxygen availability and surfactin
81 production during the growth and death of *B. subtilis* cultures. We show that oxygen
82 becomes limiting in the culture during the transition to stationary phase and that surfactin
83 secretion improves growth yield in stationary phase by increasing oxygen availability.
84 During a shift to anoxic conditions, we demonstrate that the majority of *B. subtilis* cells die
85 and lyse due to the activity of the LytC autolysin and surfactin. Finally, we discover that

86 surfactin maintains the viability of the remaining cells by causing membrane

87 depolarization that allows these cells to survive until oxygen is restored.

88 # Results

89

90 **Oxygen depletion leads to rapid death and lysis of most *B. subtilis* cells**

91 When culturing the biofilm-forming *B. subtilis* strain 3610 in LB, we noticed that once a test
92 tube containing a late exponential culture was shifted from a shaking incubator to a
93 stationary rack on the bench, the opacity of the tube decreased continuously over a period
94 of 10 hours, suggesting that cells were dying and lysing (Fig. 1A). Consistent with lysis,
95 microscopic observation of cultures left to sit on the bench for 10 hours revealed
96 substantial phase-gray cell remnants in addition to phase-dark rod-shaped cells (Fig. 1A).
97 We conclude that *B. subtilis* 3610 cultures exhibit death and lysis during static incubation
98 after cessation of rapid growth.

99 The static culture would be limited in oxygen diffusion, and as *B. subtilis* is a strict
100 aerobe that relies on its use of oxygen as a terminal electron acceptor during respiration,
101 we hypothesized that the death in the culture was due to oxygen limitation. To measure
102 oxygen levels during oxygen growth and depletion, we added phosphorescent oxygen-
103 sensitive nanoparticles (Methods) to cell cultures in microtiter plates and measured optical
104 density (OD) and light emission over time. To establish a controlled environment, we grew
105 cultures in sealed 96-well microtiter plates with a hole poked in the seal to allow oxygen
106 exchange, or limited oxygen by completely sealing the wells (Fig. 1B, top); we utilized
107 linear shaking to prevent an oxygen gradient in the culture. In media without cells, oxygen
108 initially diffused into the media due to shaking, and then remained at an approximately
109 constant value (Fig. 1B, bottom). In media with cells, oxygen levels initially increased (again
110 due to shaking) but then began to decrease when the culture reached an OD_{600}~0.05,

111 indicating that the cells were consuming the oxygen faster than it dissolved into the media
112 (Fig. 1B). When cultures reached an OD_{600}~0.5, oxygen levels were undetectable but the
113 culture continued to grow (Fig. 1B), presumably because the cells rapidly consumed any
114 oxygen that dissolved into the media.

115 When the cultures reached an OD_{600}~0.8, we sealed the wells to abolish oxygen
116 exchange in the headspace, and returned the cultures to a shaking environment. As
117 expected, the measured oxygen levels in the cultures remained low (Fig. 1B, lower right).
118 Within 2 hours, the OD_{600} began to decrease, reminiscent of our observations of OD loss in
119 standing test tubes (Fig. 1A), and plateaued at ~0.1 after 48 h (Fig. 1B, upper right).
120 Consistent with the OD drop upon sealing the well, cell viability (defined here as the ability
121 of a cell to form a colony on an agar plate) dropped approximately ten-fold after 48 h (Fig.
122 1C). These observations suggest that the loss of OD in standing tubes and in agitated sealed
123 plates was due to cell lysis during oxygen depletion.

124 To further explore the correlation between cell lysis and oxygen depletion, we
125 investigated the effect of cell density on hypoxia-induced cell lysis by growing cultures
126 aerobically to different optical densities prior to sealing the wells. Regardless of starting
127 culture density (OD_{600} from 0.4 to 0.8), the OD_{600} either stayed approximately constant or
128 increased slightly for ~1 hour after sealing, and then the cultures exhibited large decreases
129 in OD over time (Fig. 1D, S1A). The maximum lysis rate (the absolute value of the most
130 negative slope of the $\ln(OD_{600})$ curve) increased with increasing starting OD, such that the
131 cultures that began at the highest density (OD_{600}~0.8) had a lysis rate of 40% decrease per
132 hour (Fig. 1D). Since the lysis behavior varied with initial OD, we standardized all further
133 experiments by growing 3610 cells to an OD_{600} of ~0.9-1.1 before cutting off oxygen

134 exchange. Transfer of OD~1 cultures into an anaerobic chamber resulted in an even higher
135 maximum lysis rate of 86% decrease per hour (Fig. S1B). From these data, we infer that
136 populations at high density deplete the remaining oxygen more rapidly, and that rapid
137 oxygen depletion more readily triggers cell lysis.
138

139 **A cell wall autolytic enzyme is necessary for lysis of non-viable cells upon oxygen**
140 **depletion**

141 In addition to losing viability upon oxygen depletion, the non-viable population also lysed
142 and was removed from the population of intact cells, as indicated by the substantial
143 decrease in optical density. Given the importance of the cell wall for maintaining cellular
144 integrity in bacteria, we hypothesized that this lysis involves the activity of cell wall
145 autolytic enzymes. Cell wall growth requires both insertion of new material and cleavage of
146 the existing peptidoglycan by autolysins [28]. In *B. subtilis*, the major autolysin LytC is
147 under control of the vegetative sigma factor $\boldsymbol{\sigma}^{A}$ and the alternative sigma factor $\boldsymbol{\sigma}^{D}$ [29, 30],
148 preventing the unchecked breakdown of the cell wall when insertion is disrupted [31]. We
149 measured the OD of a Δ*lytC* 3610 mutant and found that the mutant exhibited reduced lysis
150 upon oxygen depletion (Fig. 1C). As a specificity control, deletion of another $\boldsymbol{\sigma}^{D}$-dependent
151 autolysin LytD phenocopied wild-type behavior (Fig. S1C), suggesting that LytC is the
152 primary autolysin activated in oxygen-depleted conditions. Despite the higher biomass in
153 the Δ*lytC* cultures after oxygen depletion, a similar proportion of cells (~10%) retained
154 viability as in wild-type cultures (Fig. 1C). Single-cell imaging of the oxygen-depleted
155 cultures revealed mixed populations of rod-shaped cells, some of which were phase-gray
156 "ghosts" and others that were phase dark (Fig. 1C). Time-lapse microscopy demonstrated

157 that only a portion of the phase-dark rod-shaped Δ*lytC* cells were capable of resuming
158 growth (Fig. S1D, movie S1, S2), consistent with our plating efficiency data (Fig. 1C). These
159 data indicate that lysis and cell viability are genetically separable phenotypes, since many
160 Δ*lytC* mutant cells remain intact yet still lose viability. Thus, since LytC degrades the cell
161 wall but does not impact the viability of 3610 cultures upon oxygen depletion, we conclude
162 that lysis is downstream of viability loss during oxygen depletion.
163

164 **Laboratory-domesticated *B. subtilis* strains exhibit more viability loss despite**
165 **reduced lysis upon oxygen depletion**

166 *B. subtilis* strain 168, a genetic derivative of 3610, is commonly used in research
167 laboratories as it was selected for dispersed growth in culture and improved genetic
168 tractability [17]. In microtiter plate assays, we found that upon oxygen depletion the OD of
169 168 cultures decreased at a lower rate and remained at a higher level throughout 48 h of
170 monitoring (Fig. 2A). Imaging of oxygen-depleted 168 cultures revealed the presence of
171 round cells in addition to rod-shaped cells (Fig. 2B). Some round cells were intact and did
172 not stain with propidium iodide (PI), while others had compromised membranes and thus
173 stained brightly with PI (Fig. 2B). In cell cultures that were first stained with fluorescent D-
174 amino acids (FDAAs) to label cell walls, the vast majority of the rounded cells did not retain
175 FDAA staining, indicating that they were protoplasts without cell walls (Fig. S2A). Indeed, a
176 168 Δ*lytC* strain did not form round cells and exhibited less lysis (Fig. S2B), indicating that
177 the protoplasts released in 168 are more fragile than their walled counterparts. Thus, we
178 conclude that LytC activity during oxygen depletion degrades the cell wall in 168, releasing

179 membrane-bound protoplasts that account for the higher OD in 168 cultures compared
180 with 3610 cultures.

181 Despite having a higher OD_{600} than 3610 cultures, the colony-forming units (CFU) in
182 168 cultures depleted of oxygen for 24 h decreased ~100-fold relative to 3610 (Fig. 2C).
183 Indeed, time-lapse imaging on fresh medium with oxygen showed that despite having
184 intact cell envelopes, only ~1% of the rod-shaped 168 cells were able to grow and divide,
185 whereas ~95% of the 3610 cells exhibited growth (Fig. S2C, Movie S3,S4). We never
186 observed growth either in increased cell number or increased cell size during 12 h time-
187 lapse imaging of any of the protoplasts on fresh LB or on filtered spent medium, suggesting
188 that the protoplasts formed in strain 168 are not viable. We conclude that despite reduced
189 cell lysis, 168 cultures experience a much more drastic loss of viability upon oxygen
190 depletion.

191

192 **Surfactin increases lysis and restores viability to the domesticated strain 168**

193 Strains 3610 and 168 differ in a number of chromosomal loci, and 168 is defective in
194 phenotypes related to secretion of extracellular products that support multicellular
195 behaviors such as biofilm formation and swarming motility [18]. To determine whether
196 extracellular products were responsible for the oxygen-related phenotypic differences
197 between the two strains, we subjected a 1:1 volumetric mixture of the strains to oxygen
198 depletion. The viability of 168 (which has a colony morphology visually distinct from that
199 of 3610) increased dramatically in the co-culture (Fig. 4C). A candidate compound that
200 could restore viability to 168 is surfactin, which is a strong surfactant that creates K^+-
201 permeable pores and solubilizes lipid bilayer vesicles *in vitro* [32]. Surfactin is produced by

202 3610 but not 168, due to a mutation in *sfp*, which encodes an enzyme necessary to activate
203 the surfactin biosynthesis complex [19]. We found that exogenous surfactin addition at
204 either the time of inoculation of the culture or at the initiation of oxygen depletion
205 increased the lysis rate of 168 and eliminated protoplasts (Fig. 2D,E), consistent with
206 surfactin-induced protoplast lysis.

207 Remarkably, exogenous surfactin addition restored the viability of oxygen-depleted
208 168 cultures to similar levels as 3610 (Fig. 2F). Moreover, a 168 strain with *sfp* genetically
209 complemented to restore surfactin production phenocopied the surfactin-treated 168
210 cultures in terms of lysis, cell morphology, and viability (Fig. 2F, S2). Thus, we conclude
211 that surfactin production both promotes protoplast lysis and maintains viability in oxygen-
212 depleted *B. subtilis* cultures.

213

214 **Surfactin improves growth yield of the domesticated strain 168 by increasing oxygen**
215 **diffusion**

216 One intriguing distinction between the aerobic growth of 3610 and 168 was the divergence
217 of the growth curves around OD_{600}~0.3; after this point, 3610 cultures completed another
218 ~1.5 mass doublings to reach OD_{600}~0.9, while 168 cultures underwent only 1 mass
219 doubling to reach OD_{600}~0.6 over the same period (Fig. 3A). We noted that a surfactin-
220 supplemented culture experienced more growth after the OD reached ~0.3 than untreated
221 cultures, resulting in a higher overall yield similar to that of 3610 (Fig. 3B). When surfactin
222 was added just prior to the divergence in growth curves, the yield was similarly restored
223 (Fig. 3B). Thus, we inferred that surfactin production was responsible for the increase in
224 yield of 3610 relative to 168. The detergent Tween 80 similarly increased growth yield in

225 168 cultures (Fig. 3C), indicating that the detergent properties of surfactin were likely
226 responsible for the increased yield.
227 Certain compounds have the ability to increase oxygen diffusion in liquid [33], and it
228 has been proposed that oxygen diffusivity is rate-limiting for the function of some
229 biological systems [34]. To test whether surfactin increased oxygen in the media, we used
230 our oxygen nanoprobe to compare oxygen levels in 168 cultures with and without added
231 surfactin. We found that exogenous surfactin increased the oxygen levels in cultures during
232 late-exponential phase, when oxygen would normally be depleted lower than our limit of
233 detection (Fig. 3D). A similar increase occurred due to addition of Tween 80 (Fig. 3D). A
234 biophysical model incorporating diffusion and cellular consumption of oxygen predicted
235 that the observed ~1.2-fold increase in peak oxygen level is consistent with a ~1.4-fold
236 increase in diffusion rate (Methods). Thus, we infer that the presence of surfactin results in
237 higher growth yield due to the enhanced availability of oxygen during the transition to
238 stationary phase when oxygen would otherwise be limiting for growth.
239
240 **A transposon screen supports surfactin production as the main determinant of**
241 **survival upon oxygen depletion**
242 Given the large decreases in viability after 24 h of oxygen depletion, we performed a
243 genetic screen to attempt to identify any mutations that would increase the survival of 168
244 and 3610 without oxygen. We made 20-30 independent transposon libraries of 5000-
245 10,000 individual transposon mutants per library in each background and subjected these
246 libraries to oxygen depletion, hypothesizing that any mutants with enhanced survival
247 would be enriched (Fig. S3A). We could not identify any such 168 mutants, suggesting that

248 there is not an easily obtainable loss-of-function mutant in a surfactin-independent
249 pathway to increase viability upon oxygen depletion.
250 We identified two categories of mutants in the 3610 background with decreased
251 lysis upon oxygen depletion: surfactin production (*comA*, *comP*, *srfAA,* and a hit upstream of
252 *rghR* (*rghR*$_{us}$)) and flagella-related (*fliI, fliJ*, and *fliF*) (Fig. S3B, Table S1). *srfAA* encodes the
253 surfactin synthetase subunit A, which is part of the enzyme that synthesizes surfactin (Fig.
254 4A) [19, 35]. ComA and ComP form a two-component system that activates surfactin
255 production at high cell density [36]. RghR regulates RapG and RapH, two repressors of the
256 *srfA* operon (Fig 4A) [37]. The flagella-related mutants disrupted *fliI* and *fliJ*, which encode
257 accessories of the flagellar type III secretion apparatus, and *fliF*, which encodes the flagellar
258 basal ring [38-41]. In-frame markerless deletions of these mutants had ~4-fold lower
259 viability than the parent after 24 h of oxygen depletion (Fig. S3C), which we hypothesized
260 was due to the surfactin in the pooled library cultures increasing their survival advantage
261 in the mixed population but not in isolation. Indeed, upon exogenous surfactin addition, all
262 mutants responded with increased lysis and removal of protoplasts/cell debris (Fig. 4B,C,
263 S3D). Taken together, the fact that we obtained no hits that increased viability in a 168
264 background and that all hits in a 3610 background are directly related to surfactin
265 production or respond to surfactin points to surfactin as the primary determinant of
266 viability in the absence of oxygen.
267

268 **Surfactin restores viability by depolarizing the membrane**

269 *In vitro*, surfactin creates potassium ion-permeable pores in lipid bilayers [32]. If this
270 behavior occurs *in vivo*, such pores would reduce the strength of the potassium ion

271 gradient across the cell membrane and alter membrane potential. Thus, we tested the
272 energetic state of cells after various chemical treatments using the membrane potential-
273 sensitive dyes $DiSC_3(5)$ and ThT [42, 43]. $DiSC_3(5)$ is taken up by cells and the fluorescence
274 signal is initially quenched. Agents that depolarize cells release $DiSC_3(5)$ into the medium,
275 resulting in an increased signal [42]. By contrast, ThT enters cells with polarized
276 membranes and fluoresces inside the cell; upon depolarization, ThT exits the cells and the
277 fluorescence is reduced [43]. As expected, we found that treatment of 168 cells with
278 valinomycin, a known depolarizing agent that functions as a potassium-specific transporter
279 [44], led to an increase in $DiSC_3(5)$ and a decrease in ThT signal (Fig. 5A). CCCP, a proton
280 ionophore that dissipates the proton motive force [45], strongly reduced the ThT signal
281 and slightly increased $DiSC_3(5)$ fluorescence (Fig. S4). Surfactin treatment led to a large
282 increase in $DiSC_3(5)$ fluorescence and a greater decrease in ThT fluorescence than
283 valinomycin (Fig. 5A), demonstrating that surfactin can strongly depolarize *B. subtilis* cells.
284 Based on these findings, we hypothesized that de-energizing the membrane would
285 be sufficient to rescue the colony-forming ability of 168 cultures upon oxygen depletion.
286 Indeed, valinomycin and CCCP both restored viability to a similar extent as surfactin (Fig.
287 5B). Interestingly, valinomycin- and CCCP-treated cultures had protoplasts after 24 h of
288 oxygen depletion, consistent with surfactin being necessary for protoplast lysis and
289 indicating that protoplast formation is independent from viability maintenance. Taken
290 together, these data indicate that membrane potential dictates the ability of *B. subtilis* cells
291 to survive oxygen depletion.

292 **Discussion**

293

294 While surfactin has been recognized to promote swarming motility and complex colony
295 architecture in *B. subtilis* communities such as biofilms [18, 46], its role in planktonic
296 cultures has remained mysterious. Here, we demonstrate three independent roles of
297 surfactin in planktonic cultures. During aerobic growth, the detergent properties of
298 surfactin increase growth yield by increasing the oxygen available to cells entering
299 stationary phase (Fig. 3). During oxygen depletion, surfactin plays two independent roles:
300 (1) it works in tandem with LytC to remove non-viable cells from the culture (Fig. 2), and
301 (2) it depolarizes the remaining cells and thereby maintains their viability during oxygen
302 depletion (Fig. 5).

303 The increase in growth yield due to surfactin suggests that oxygen is limiting even in
304 aerobic cultures and that increasing oxygen availability can increase yield. This finding has
305 industrial implications as *B. subtilis* is commonly used to produce many biological
306 compounds such as enzymes and antibiotics [47], and maintaining oxygen levels are critical
307 to optimize production of the desired compound [48, 49]. If this oxygen-related growth
308 yield enhancement holds across species, detergent addition may increase bioproduction in
309 other commonly utilized organisms such as *Streptomycetes* species, which are used to
310 isolate numerous antibiotics, and the industrial powerhouse *Escherichia coli*, which is
311 widely used to synthesize many biopharmaceuticals such as insulin [47]. In addition to
312 oxygen, surfactin may also facilitate growth by increasing nutrient diffusion to cells during
313 late exponential phase when nutrients become limiting.

314 We also found that surfactin has at least two functions during oxygen starvation that
315 are distinct from its role during aerobic growth. Surfactin causes lysis in cells that
316 experience LytC-mediated cell wall degradation (Fig. S2), presumably through membrane
317 disruption. Moreover, surfactin maintains viability of the remaining intact cells through
318 membrane depolarization, which may allow these cells to enter a metabolically inactive
319 state where they can ride out the stress of the oxygen depletion. While it was formally
320 possible that cell lysis helped maintain viability of the remaining cells, the observations
321 that Δ*lytC* mutants have the same viability as wild-type cultures even though the non-viable
322 cells remain intact (Fig. 1C) and that CCCP or valinomycin treatment of 168 cultures
323 rescues viability without removing protoplasts (Fig. 5C) demonstrate that surfactin
324 maintains viability by acting directly upon the membrane potential of the surviving cells.
325 Generally, OD is used as a proxy for cell number, which holds true for our
326 measurements of 3610 cultures undergoing oxygen depletion as the 10-fold drop in OD
327 measured reflects cell lysis and quantitatively mirrors the decrease in viability (Fig. 1C).
328 However, our work highlights instances during oxygen depletion when biomass measured
329 by OD is uncoupled from viability: both Δ*lytC* 3610 cells and 168 cells remain intact and the
330 cultures have a relatively high OD compared with wild-type 3610, but most cells cannot
331 form colonies (Fig. 2C, S1C). This uncoupling between OD and viability has been observed
332 previously in cell-cycle mutants where cells remain intact and metabolically active but
333 cannot divide and form colonies [51], and may be more prevalent than is currently
334 appreciated, motivating future studies that rely on OD to perform assays to verify culture
335 viability.

336 Since cell depolarization can actually improve the viability of cells undergoing
337 oxygen depletion, under conditions with limiting terminal electron acceptors, certain
338 antibacterial treatments that inhibit growth may actually keep cells viable. Such a
339 possibility needs to be taken into consideration when treating bacterial infections and
340 removing bacteria in low-oxygen clinical and industrial settings, particularly those in which
341 the microbe primarily gains energy through aerobic respiration and hence the terminal
342 electron acceptor may be limiting. Moreover, it remains generally unclear which
343 antimicrobial treatments will disrupt membrane potential as a side effect of their primary
344 activity or mechanistically how antibiotic treatments affect cells in low oxygen
345 environments, motivating further studies of membrane energetics during growth-
346 inhibition.
347 The cell-wall breakdown of *B. subtilis* cells during oxygen depletion provides further
348 support for a recently discovered regulatory role of membrane potential in cell-wall
349 synthesis [52]. Indeed, LytC is activated upon sodium azide treatment that deprotonates
350 the cell wall [53, 54] and the activity of peptidoglycan synthesis enzymes in *E. coli* are
351 regulated by pH [55, 56]. In addition, the recent observation that actively growing and
352 dormant cells in a *B. subtilis* culture respond oppositely to an electrical pulse wherein they
353 either hyperpolarize or depolarize, respectively [57], suggests that membrane energetics
354 may explain the observed population heterogeneity in our oxygen-depleted 3610 cultures.
355 Thus, as membrane potential is of utmost importance in metabolism and cell growth, is
356 becoming more appreciated in regulating cell-wall remodeling, and likely feeds back into
357 many additional aspects of cell physiology, bacteria must employ strategies to maintain
358 and/or modulate membrane potential during changing environmental conditions. The

359 ability of surfactin to both alter membrane energetics to maintain viability during oxygen-
360 depletion and to enhance growth in oxygen-limited conditions has likely provided multiple
361 fitness advantages to *B. subtilis* in spatially structured and complex environments such as
362 native soil communities, and strategies for regulating membrane potential may be an
363 important factor for survival of other strict aerobes as well.

364 **Methods**

365

366 **Media and growth conditions**

367 All strains and their genotypes are listed in Table S2. Strains were grown in LB (Lennox
368 broth with 10 g/L tryptone, 5 g/L NaCl, and 5 g/L yeast extract). Antibiotics for selection of
369 mutant strains were used as follows: kanamycin (5 μg/mL), MLS (a combination of
370 erythromycin at 0.5 μg/mL and lincomycin at 12.5 μg/mL), chloramphenicol (5 μg/mL),
371 and spectinomycin (100 μg/mL). Surfactin was added at a final concentration of 0.05
372 mg/mL unless otherwise noted. Strains were cultured either in 5 mL of medium in a test
373 tube on a roller drum or in 200 μL of medium in a 96-well plate in a Biotek Epoch2
374 spectrophotometer under linear shaking (shaking was set to 567 cycles per minute (cpm),
375 3-mm magnitude of shaking). For all experiments, the initial inoculum was from a fresh
376 colony struck from a -80 °C freezer stock onto LB 1.5% agar plates and incubated overnight
377 at 37 °C.

378

379 **Strain construction**

380 Strains were constructed using SPP1 phage transduction [58]. The donor strain was grown
381 for >6 h in TY medium (LB supplemented with 0.01 M $MgSO_4$ and 0.1 mM $MnSO_4$ after
382 autoclaving). Ten-fold dilutions of SPP1 phage were added to the culture and 3 mL TY soft
383 (0.5%) agar was mixed with the culture/phage mixture and poured over a TY plate (1.5%
384 agar) overnight. A plate was chosen that exhibited nearly total clearing of cells without a
385 large number of phage-resistant mutants. Five milliliters of TY medium were added to this
386 plate and a 1-mL filter tip was used to scrape up the soft agar. This soft agar/liquid mix was

387 filtered through a 0.4-μm filter. The phage was added to a stationary-phase (grown for 6-10
388 h) culture in TY medium of the recipient strain (10 μL undiluted phage + 100 μL recipient
389 cells, and optionally 900 μL TY medium) and incubated at 37 °C for 30 min, then plated
390 onto LB + antibiotic and 0.01 M sodium citrate (sodium citrate was omitted for MLS
391 selection). Plates were incubated for 24 h and transductants were struck for single colonies
392 to eliminate the phage.

393 To generate the Δ*lytC* in-frame marker-less deletion construct, the region upstream
394 of *lytC* was PCR-amplified using the primer pair 1427/1428 and digested with SalI and
395 EagI, and the region downstream of *lytC* was PCR-amplified using the primer pair
396 1425/1426 and digested with EagI and BamHI. The two fragments were then
397 simultaneously ligated into the SalI and BamHI sites of pMiniMAD, which carries a
398 temperature-sensitive origin of replication and an erythromycin resistance cassette [59], to
399 generate pDP299.

400 To generate the Δ*lytD* in-frame marker-less deletion construct, the region upstream
401 of *lytD* was PCR-amplified using the primer pair 1429/1430 and digested with SalI and
402 EagI, and the region downstream of *lytD* was PCR-amplified using the primer pair
403 1431/1432 and digested with EagI and BamHI. The two fragments were then
404 simultaneously ligated into the SalI and BamHI sites of pMiniMAD to generate pDP300.

405 Deletion plasmids were introduced into strain DK1042 (Table S2) via single cross-
406 over integration by transformation at the restrictive temperature for plasmid replication
407 (37 °C) using MLS resistance as a selection. To evict the plasmid, the strain was incubated
408 in 3 mL LB broth at a permissive temperature for plasmid replication (22 °C) for 14 h, and
409 serially diluted and plated on LB agar at 37 °C. Individual colonies were patched on LB

410 plates and LB plates containing MLS to identify MLS-sensitive colonies that had evicted the
411 plasmid. Chromosomal DNA from colonies that had evicted the plasmid was purified and
412 screened by PCR using primers 1427/1426 or 1430/1431 to determine isolates that had
413 retained the Δ*lytC* or Δ*lytD* allele, respectively [59, 60].

414 In-frame deletions of MLS-knockout mutants were constructed as outlined
415 previously [14]. Briefly, the strain of interest was transformed with pDR244 at 30 °C.
416 Several transformants were struck onto LB at 42 °C. Resultant colonies were patched on
417 MLS and spectinomycin plates to confirm that the plasmid and MLS cassette were lost.
418 Colonies were screened for altered oxygen phenotype.

419

420 **Growth and lysis assays**

421 Strains were struck out for single colonies on the evening prior to the experiment. Colonies
422 were inoculated into fresh LB and grown aerobically at 37 °C, either in 5 mL LB on a roller
423 drum or in 200 μL in a Greiner 96-well plate. To deplete oxygen from cultures grown in test
424 tubes, 200 μL were aliquoted into a 96-well plate and the plate was sealed with optical film
425 (Excel Scientific AeraSeal). To grow cultures in the plate reader, 200 μL of stationary-phase
426 inocula were aliquoted into each well of a 96-well plate, with the edge wells containing
427 medium only. Optical film was used to cover the plates, and one hole per well was poked
428 using a 20-gauge needle to allow for air exchange. 168 and 3610 cultures were then grown
429 until the 3610 culture reached an OD_{600}~1.0. To deplete the oxygen, the plate was taken
430 out of the plate reader, the optical seal with holes was removed, and a new seal was placed
431 onto the plate to fully cut off oxygen exchange. We grew and depleted cultures at 37 °C

432 using linear shaking (567 cpm, 3-mm magnitude) and read OD_{600} every 7.5 min in a Biotek
433 Epoch2 spectrophotometer.
434
435 **Mariner transposon library construction**
436 The mariner transposon was used to create a library of insertion mutants. The parent
437 strains (HA1235 and HA1414) were struck for single colonies onto MLS plates at 30 °C. One
438 colony per library was grown in 3 mL LB+kanamycin at room temperature overnight.
439 Transposon-insertion libraries were selected by plating 10-fold dilutions of the cultures on
440 prewarmed LB+kanamycin plates and incubating overnight at 37 °C.
441
442 **Screen to enhance for mutants that survive better without oxygen**
443 Each library (~5000-10,000 colonies per library) was inoculated into 5 mL LB and grown
444 on a roller drum at 37 °C to an OD_{600}~1.0. Libraries were then aliquoted into wells of a 96-
445 well plate (200 μL per well) and plates were sealed to deplete oxygen. Oxygen was
446 depleted at 37 °C for 2-8 days for 168 libraries or at 30 °C for 4-8 days for 3610 libraries. At
447 various time points following the start of oxygen depletion, one well of the library was
448 harvested and struck out for single colonies. One or two colonies per well were tested for
449 either enhanced lysis upon oxygen depletion (3610 background) or enhanced colony-
450 forming ability (168 background). Any mutants found to have these phenotypes were back-
451 crossed into the parent using SPP1 phage transduction to ensure the transposon mutation
452 was the causative agent. To map the mutation, genomic DNA was prepped from each
453 mutant. Inverse PCR was carried out using Phusion polymerase with the primers IPCR1

454 and IPCR2. The PCR products were gel-purified and sequenced using the IPCR2 primer. The
455 sequences were mapped onto the *B. subtilis* genome using BLASTN.
456
457 **Oxygen nanoprobe measurements**
458 Relative oxygen levels were measured using the oxygen-sensitive nanoprobe
459 (BF_2nbm(I)PLA) that emits an oxygen-dependent phosphorescence reading and an oxygen-
460 independent fluorescence reading, which together can be used to calculate the relative
461 oxygen level of the medium [61, 62]. Briefly, the nanoprobe was added at 5% (10 μL into
462 190 μL) to the inoculum before growth of the cultures. In addition to OD_{600} readings,
463 fluorescence readings (ex/em: 414/450 nm) and phosphorescence readings (ex/em:
464 415/560 nm, with a 2-ms delay between excitation and emission) were taken using a
465 Biotek Synergy H1 spectrophotometer. Readings were taken every 7.5 min, with incubation
466 at 37 °C and linear shaking (567 cpm, 3-mm magnitude of shaking).
467
468 **PI staining and phase microscopy**
469 Five hundred nanoliters of cultures were spotted onto LB pads made with 1.5% agar and
470 10 μM PI. Once dry, a coverslip was added and cells were imaged on a Nikon Ti-E inverted
471 microscope using a 100X objective (NA: 1.4). Phase and fluorescence (mCherry filter,
472 ex/em: 570/645 nm) images were acquired. Images were processed identically in Adobe
473 Photoshop and merged using FIJI.
474
475 **Time-lapse microscopy of oxygen-depleted cultures**

476 The bottom of a rectangular Singer PlusPlate culture plate was used to make a large pad
477 [63], in which 35 mL of LB+1.5% agar was pipetted onto the plate ~1 h before imaging so
478 that the agar could solidify completely. Once solid (after ~5-10 min), a second Singer
479 PlusPlate was placed on top of the agar pad to prevent contamination and drying. One
480 microliter of cultures was spotted in the center of the pad and allowed to dry. A large 113
481 by 77 mm custom-made no. 1.5 glass coverslip (Nexterion) was applied [63]. Imaging was
482 carried out in a heated environmental chamber with a water bubbler and several
483 reservoirs of water to humidify the chamber. Phase images were acquired on a Nikon Ti-E
484 inverted microscope every 5 min using a 40X air objective (NA: 0.95) with 1.5X
485 magnification. Images were compiled into movies and analyzed using Matlab or FIJI. All
486 rod-shaped cells were identified in the first frame and defined as able to grow if they at
487 least doubled in mass and divided without lysis during the experiment.
488
489 **Fluorescent D-amino acid staining**
490 HADA [64] was added to cultures at a final concentration of 500 μM during the last mass
491 doubling of growth. To reduce background staining, cultures were diluted 1:10 in MSgg
492 solution (5 mM potassium phosphate buffer + 0.05 M MOPS at pH 7) and then spotted onto
493 a pad of that solution made with 1.5% agar. Cells were imaged using a Nikon Ti-E inverted
494 microscope with a 100X oil objective (NA: 1.4). Phase and fluorescence (DAPI filter, ex/em:
495 375/460 nm, exposure time 2 s) images were acquired. Phase and fluorescence images
496 were adjusted identically in Adobe Photoshop and merged in FIJI.
497
498 **Plating efficiency**

499 Cultures were harvested and diluted 10-fold into LB. One hundred microliters of the
500 dilutions were plated onto an LB plate. These plates were incubated overnight at 37 °C in a
501 single layer (not stacked). CFU/mL values of the original culture were calculated from the
502 colony counts of the dilutions that had distinct colonies.
503
504 **Lysis assay starting at different optical densities**
505 Three colonies were inoculated into a single 10 mL LB culture and mixed well. Six two-fold
506 serial dilutions of the culture were carried out and 5 mL of each dilution were transferred
507 to a test tube and incubated at 37 °C on a roller drum until the undiluted culture reached an
508 OD_{600}~0.8. Two hundred microliters of each culture were then aliquoted into a 96-well
509 plate, the plate was sealed with optical film, and OD_{600} was monitored in a Biotek Epoch2
510 spectrophotometer.
511
512 **Oxygen depletion in an anaerobic chamber**
513 Cultures were grown in aerobic conditions (96-well plate sealed with optical film, with
514 holes poked through the film for each well). Cultures were then transferred into a Coy
515 anaerobic chamber and OD_{600} was monitored using a Biotek Epoch2 spectrophotometer as
516 above.
517
518 **Biophysical model linking oxygen diffusivity and concentration in a growing culture**
519 Since the addition of surfactin increased oxygen levels in late-exponential phase of a
520 growing culture (Fig. 3D), we sought to understand whether oxygen diffusivity could
521 explain the increase. In a small region of extent Δl at a depth l below the air-liquid interface

522 of the culture, oxygen is depleted at a rate $\gamma \times \rho(l) \times c(l)\Delta l$, where γ is the absorption rate
523 per unit oxygen in close proximity to a cell, $\rho(l)$ is the cell density at depth l, and $c(l)$ is the
524 oxygen concentration at depth l. At steady state, the rate of oxygen uptake in the region of
525 extent Δl must be balanced by the rate of supply via diffusion, that is

526 $$D\frac{\partial^2 c}{\partial l^2}\Delta l = \gamma\rho c\Delta l, \qquad (1)$$

527 where D is the diffusivity of oxygen. The solution to Eq. 1 is $c(l) = c_0 e^{-l\sqrt{\gamma\rho/D}}$, assuming
528 that c_0 is the oxygen concentration at the surface, $c \to 0$ as $l \to \infty$, and $\gamma\rho/D$ is independent
529 of l. Hence, as D increases, oxygen reaches increased depths as $\sim \sqrt{D/\gamma\rho}$, and the total
530 amount of oxygen in the culture increases as $\int c(l)dl = c_0\sqrt{D/\gamma\rho}$. Thus, a 1.2-fold increase
531 in the total amount of oxygen corresponds to a 1.4-fold increase in D of $\sim$ 1.4-fold,
532 assuming that c_0 is linked to solubility and γ and ρ remain approximately constant.
533

534 **Membrane potential measurements**

535 Membrane potential was measured using a protocol modified from [42]. Cells were grown
536 in 5 mL LB in a roller drum to OD_{600}~1. Cells were washed in a buffer containing 10 mM
537 potassium phosphate, 5 mM MgSO4, and 250 mM sucrose (pH 7.0) and then resuspended
538 to a calculated OD_{600} of 0.085 in that same buffer (pelleting steps were at 5100 rcf for 3
539 min). Two hundred microliters of this mixture were added to wells in a 96-well plate. 1 μM
540 DiSC3(5) or 10 μM Thioflavin T (ThT) were added to the wells. Fluorescence readings
541 (em/ex: 620/685 for DISC and 450/482 for ThT) were taken every 12 s with 5 s of linear
542 shaking (567 cpm, 3-mm magnitude) on a Biotek Synergy H1 spectrophotometer. Readings

543 were collected for ~3 min before the drug was added and then readings were collected for

544 another 10 min.

545

546 **Acknowledgements**

547 The authors thank Alfred Spormann, Kyler Lugo, and the Huang lab for helpful discussions,
548 Chao Jiang for help with strain construction, and Maya Farha and Eric Brown for help with
549 membrane potential measurements. The authors acknowledge support from the Allen
550 Discovery Center at Stanford on Systems Modeling of Infection (to H.A.A. and K.C.H.),
551 National Institutes of Health (NIH) grants R35 GM131783 (to C.M.D. and D.B.K.) and R01
552 CA167250 (to C.A.D. and C.L.F.), and the Stanford Summer Research Amgen Scholars
553 Program (to L.V.). K.C.H. is a Chan Zuckerberg Biohub Investigator.

Figure Legends

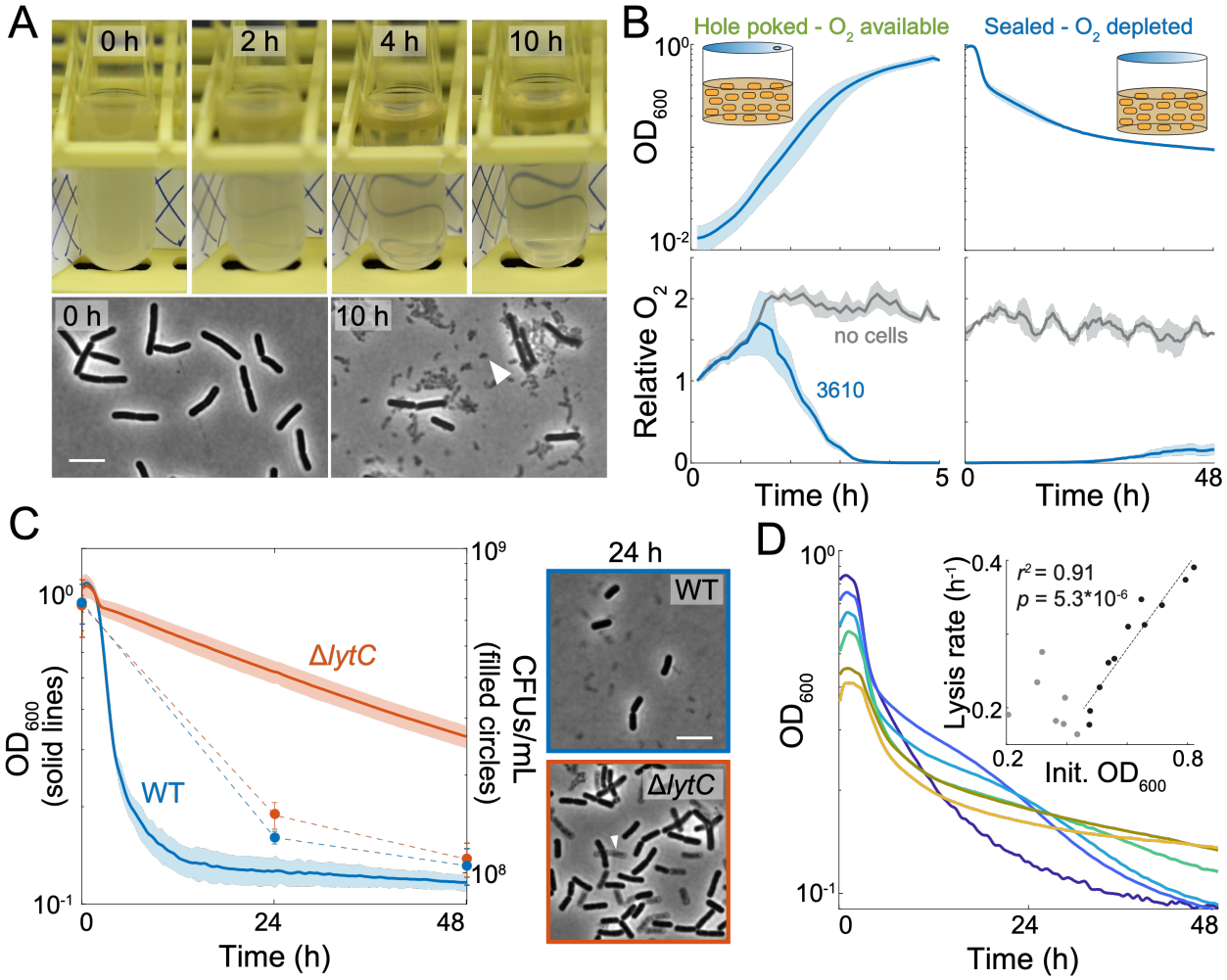

Figure 1: *B. subtilis* 3610 lyses due to oxygen depletion.

(A) *B. subtilis* cultures lyse when not shaking. Wild-type strain 3610 (WT) was grown in a test tube and then incubated at room temperature without shaking for 10 h. Phase-contrast images were acquired at 0 and 10 h. Scale bar: 5 μm; arrowhead points to cell debris.

(B) Oxygen is depleted during exponential growth and remains low throughout subsequent oxygen depletion while cultures are sealed. Cells were cultured with oxygen-sensitive nanoparticles (Methods). OD_{600} (top) and the relative oxygen

564 levels (bottom, oxygen level at first timepoint normalized to 1) of the cultures were
565 measured. Lines represent the average and shading represents one standard
566 deviation (SD), n=3.
567 (C) LytC is necessary for lysis. Left: cultures were grown to an OD_{600}~1 and then oxygen
568 was depleted at t=0 h and OD_{600} was monitored. Shading represents 1 SD, n=3.
569 Despite the differences in OD, the Δ*lytC* 3610 mutant has similar viability to wild
570 type (p=0.07 at 24 h and 0.67 at 48 h, Student's t-test). Right: phase-contrast images
571 of wild-type and Δ*lytC* cells at 24 h post-oxygen depletion. Scale bar: 5 μm;
572 arrowhead points to phase-gray, lysed cell.
573 (D) Culture lysis is strongly correlated with initial cell density when the initial
574 OD_{600}>0.45. Representative lysis curves of 6 cultures that vary in initial OD_{600} (see
575 Fig. S1 for other independent replicates). Inset: the maximum lysis rate vs. initial
576 OD_{600}. A linear regression analysis was performed on all data with initial
577 OD_{600}>0.45.

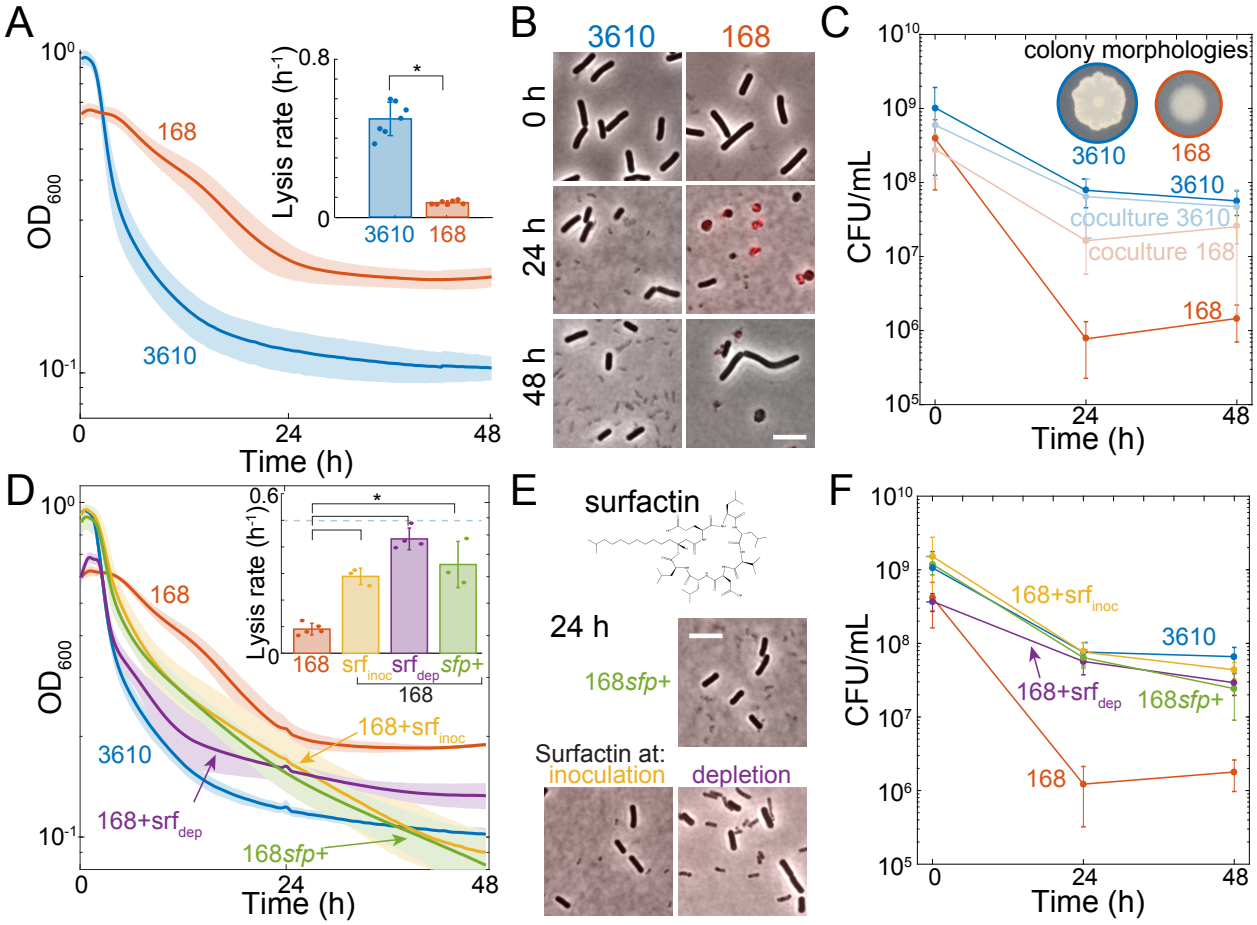

Figure 2: Surfactin production is necessary to maintain viability.

(A) *B. subtilis* strain 168 lyses less upon oxygen depletion than 3610. *B. subtilis* 3610 and 168 strains were grown aerobically and then depleted for oxygen at 0 h. Lines represent the average and shading represents 1 SD, n=7. Inset: maximum lysis rate of 3610 culture is significantly higher than that of 168 (*: p=1.7×10^{-8}, Student's t-test; Methods). Circles show individual experiment values, and error bars represent 1 SD.

(B) Many 168 cells form cell-wall-less protoplasts upon oxygen depletion. Merge of phase-contrast and fluorescence images of propidium iodide (PI)-stained cells at 0, 24, and 48 h post oxygen depletion. Red indicates membrane-compromised cells.

589 (C) Co-culturing 168 with 3610 rescues its viability upon oxygen depletion. 168
590 viability in monoculture is significantly different than 3610 (*: $p<0.005$; student's t-
591 test). Inset: 3610 and 168 have distinct colony morphologies when plated on LB.
592 Error bars represent 1 SD, n=3-5.
593 (D) Culturing with exogenous surfactin increases lysis of 168 cultures upon oxygen
594 depletion. OD curves during oxygen depletion of 3610, 168, and 168 genetically
595 rescued for surfactin production (168*sfp*+) or with 48 μM exogenous surfactin
596 added before growth (srf_{inoc}) or at depletion (srf_{dep}). Lines represent the average
597 and shading represents 1 SD, n=3-5. Inset: maximum lysis rates (*: p <0.001;
598 Student's t-test).
599 (E) Culturing with exogenous surfactin eliminates protoplasts from 168. Top: surfactin
600 molecular structure. Bottom: phase-contrast and PI fluorescence imaging at 24 h
601 post-oxygen depletion of 168*sfp*+ cells or with exogenous surfactin.
602 (F) Surfactin restores the viability of 168 cultures to near 3610 levels upon oxygen
603 depletion. Error bars represent 1 SD, n = 3-5. Surfactin-treated 168 (srf_{inoc}, srf_{dep},
604 and 168*sfp*+) cultures are each significantly different than 168 ($p<0.001$ at 24 h,
605 $p<0.01$ at 48 h, Student's t-test). By contrast, the viability of surfactin-treated 168
606 cultures are not significantly different than that of 3610 at 24 h ($p>0.2$, Student's t-
607 test).

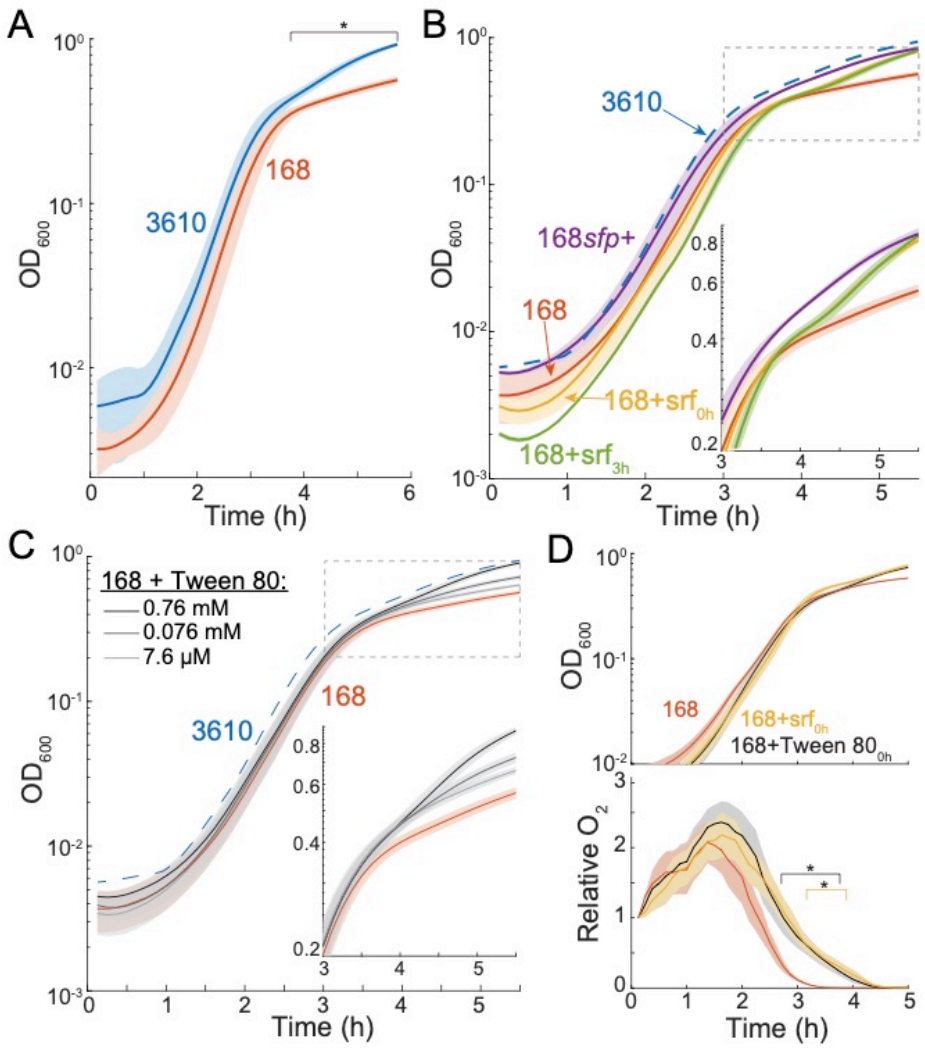

Figure 3: Surfactin restores the growth yield of 168 due to its detergent properties.

(A) 3610 aerobic cultures achieve a higher growth yield than 168. Lines represent the average and shading represents 1 SD, n=3. *: time period over which 168 growth differed significantly from that of 3610 (p<0.05, Student's t-test).

(B) Surfactin addition rescues growth yield. Growth curves of 168 with surfactin restored genetically (168*sfp*+) or 48 μM added exogenously at inoculation (168+srf$_{0h}$) or at t = 3 h (168+srf$_{3h}$). Lines represent the average and shading represents 1 SD, n=3. The mean 3610 growth curve from (A) is shown as dotted blue line. Inset: zoom-in to the period of growth divergence.

618 (C) Tween 80 addition rescues growth yield in a concentration-dependent manner.
619 Lines represent the average and shading represents 1 SD, n=3. The mean 3610
620 growth curve from (A) is shown as dotted blue line. Inset: zoom-in to the period of
621 growth divergence.
622 (D) Surfactin addition increases oxygen levels during late exponential phase. Relative
623 oxygen levels (bottom) during growth (top) of 168 with surfactin (48 μM) or Tween
624 80 (0.76 mM) added. *: time period over which oxygen levels of 168+surfactin
625 (yellow) or 168+Tween 80 (black) were significantly different from 168 cultures
626 (p<0.05, Student's t-test).

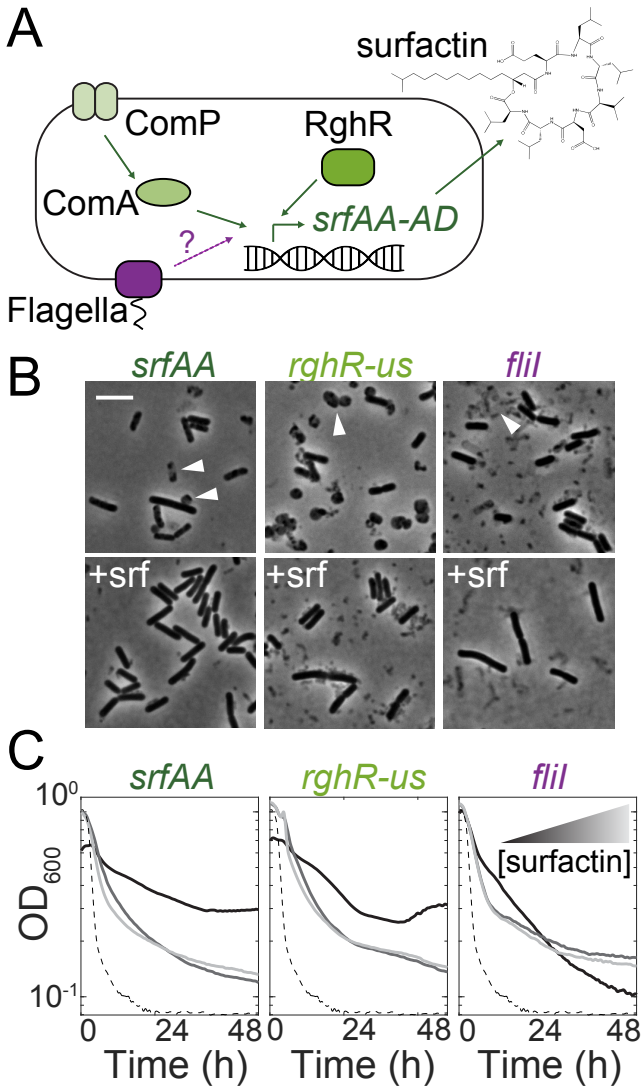

Figure 4: Transposon mutagenesis identifies genes that impact lysis during oxygen depletion.

(A) Schematic of regulation of the surfactin synthetase gene operon (*srfAA-AD*). Known regulators of SrfAA are shown in green. Our data suggests flagellar proteins (purple) may also regulate surfactin.

(B) Surfactin-treated cultures of the transposon-disrupted mutants have fewer protoplasts and cell debris. Phase-contrast images of mutants depleted of oxygen for 24 h with and without 48 μM exogenous surfactin. Top: arrowheads show

636 protoplasts, phase-gray dead cells, and cell debris, all of which were not observed in
637 the surfactin-treated cultures.
638 (C) Transposon hits exhibit faster lysis when treated with exogenous surfactin. Black
639 curves are without surfactin, medium and light gray curves are with 24 μM and 48
640 μM surfactin, respectively. The dashed line is the parent (3610).

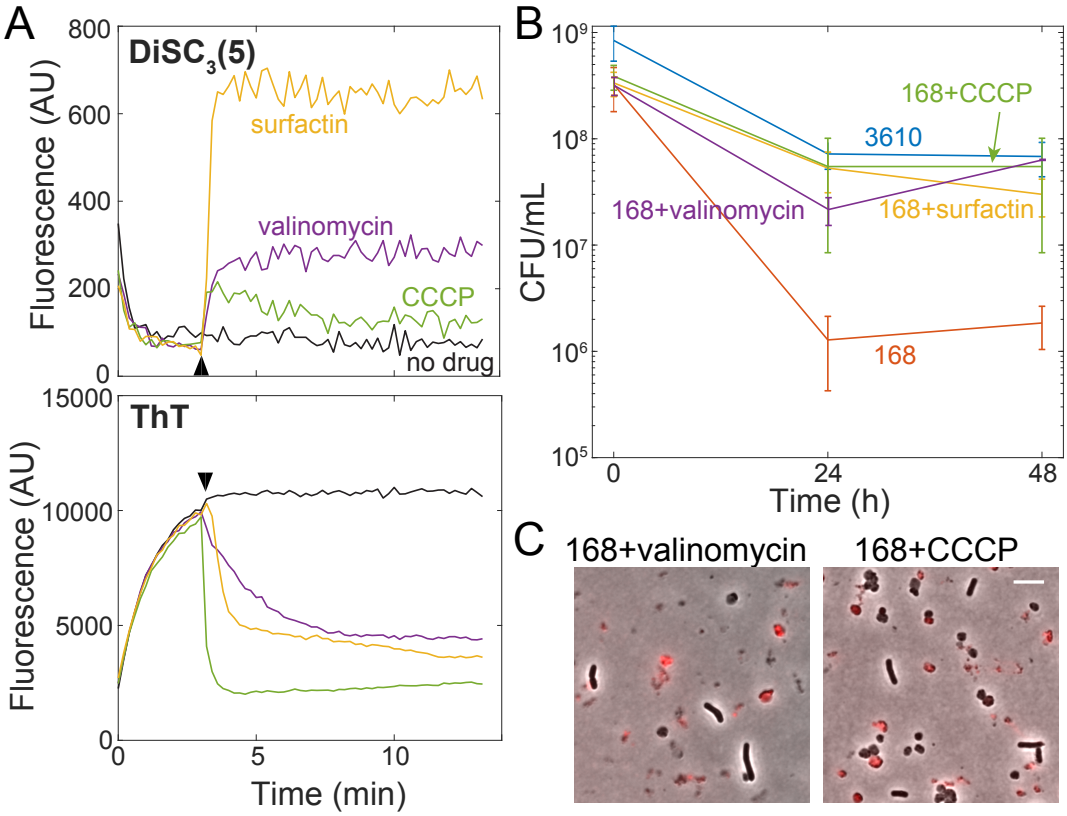

Figure 5: Surfactin maintains viability upon oxygen depletion by depolarizing the membrane.

(A) Surfactin depolarizes the membrane in *B. subtilis*. Membrane potential assays of 168 cells using the dyes $DiSC_3(5)$ (top) and ThT (bottom). The time of addition of surfactin (48 μM), valinomycin (50 μM) and CCCP (5 μM) is marked by the black arrowhead. One representative experimental replicate is shown (other replicates are in Fig. S4).

(B) Treatment with the membrane depolarizing agents valinomycin (5 μM) and CCCP (5 μM) restore plating efficiency of *B. subtilis* 168 after oxygen depletion, similar to surfactin (48 μM). Error bars represent 1 SD, n=3-5. 168 plating efficiency data are significantly different than those of 168+surfactin, 168+valinomycin, 168+CCCP, and 3610 (p<0.005, Student's t-test).

654 (C) Valinomycin and CCCP-treated 168 cultures exhibit protoplasts, demonstrating that
655 protoplast removal is not necessary for viability enhancement. Overlays of phase-
656 contrast and PI fluorescence (red) images at 24 h post-oxygen depletion. Scale bar:
657 5 μm.
658

659 **Supplemental Figures**

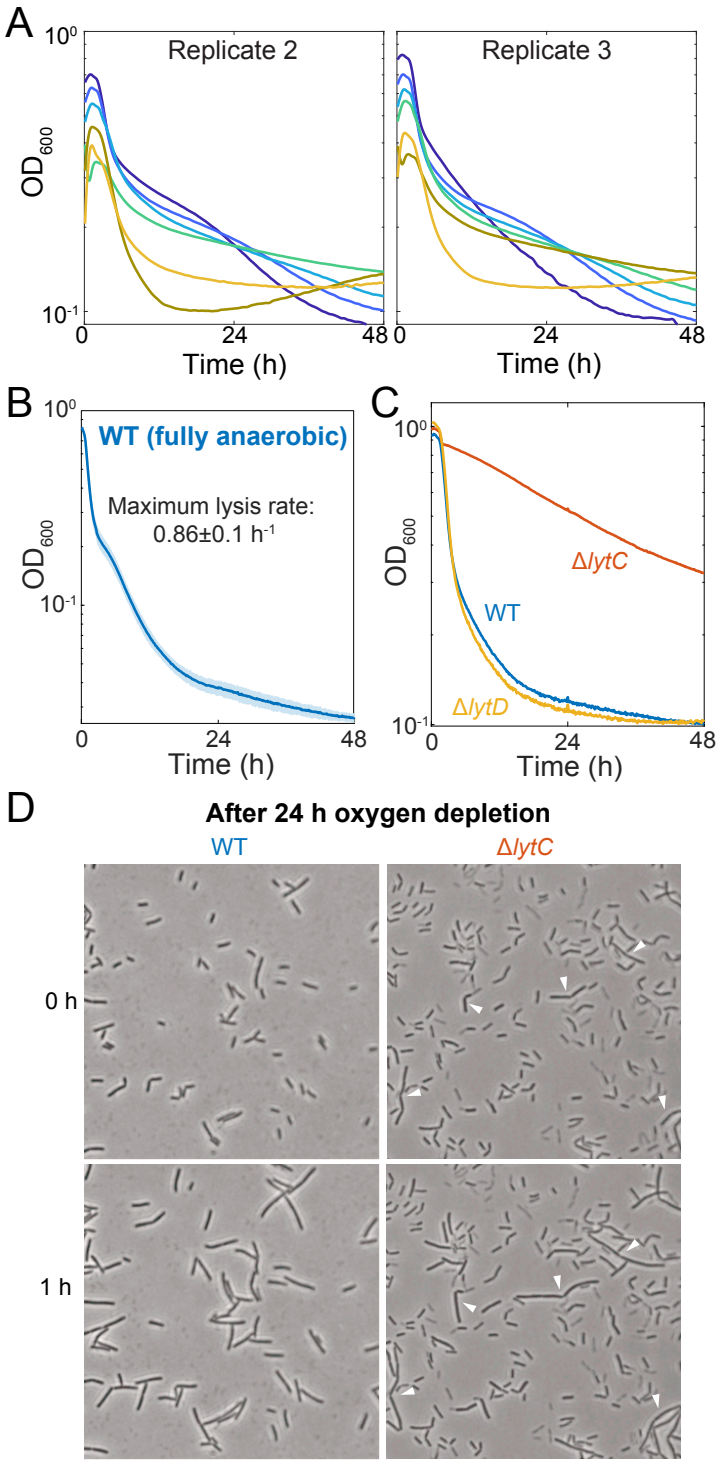

660

661 **Figure S1: Characterization of depletion in an anaerobic chamber and of Δ*lytC* and**

662 **Δ*lytD* mutants. (Related to Figure 1)**

663 (A) Culture lysis depends on cell density at the time of oxygen depletion. Two sets of
664 independent lysis curves that vary in initial OD_{600} are shown; see Fig. 1D for the
665 other independent experiments.
666 (B) Cell lysis is more rapid under anaerobic conditions. Cultures were grown in 96-well
667 plates to an OD_{600}~1 and then transferred to an anaerobic chamber to rapidly
668 remove oxygen from the culture. Line represents the average and shading
669 represents 1 SD, n=3.
670 (C) Δ*lytD* cells show similar rates of lysis to wild-type (WT) 3610 cells upon oxygen
671 depletion, unlike Δ*lytC* cells that exhibit slower lysis. Strains were grown to an
672 OD600 ~1 and then oxygen was depleted at t = 0.
673 (D) After oxygen-depletion, the majority of WT cells but only a small subset of Δ*lytC*
674 cells resume growth. After 24 h of oxygen depletion, WT and Δ*lytC* cultures were
675 spotted onto an LB pad with oxygen and cell growth was monitored. Nearly all WT
676 cells grew but only a few Δ*lytC* cells grew (arrowheads). Images shown are frames
677 from Supplemental movies 1 and 2.

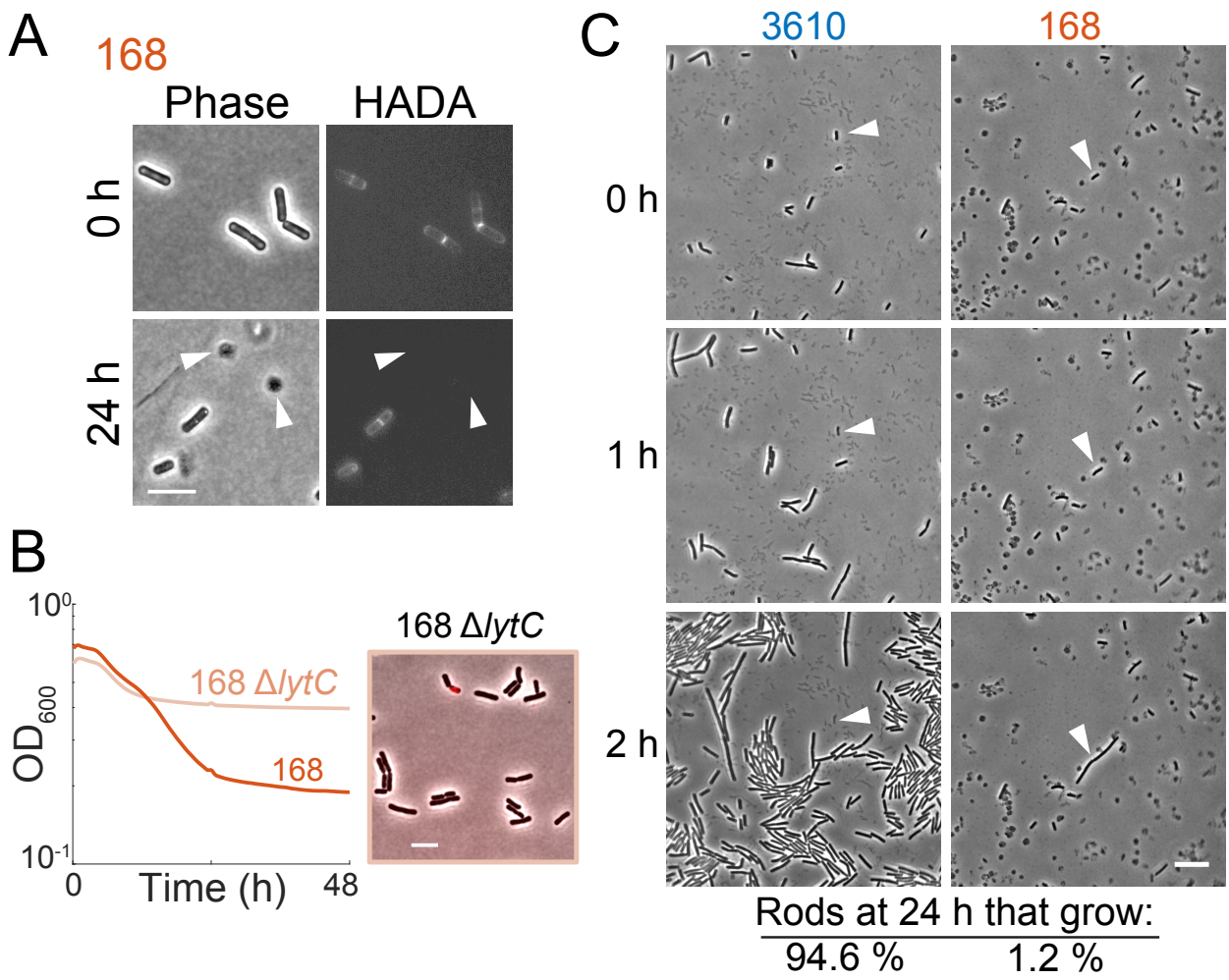

Figure S2: Oxygen depletion causes production of wall-less protoplasts in 168 and a low percentage of cells that are able to resume growth. (Related to Figure 2)

(A) Cell-wall staining reveals that protoplasts have lost their cell wall. Phase-contrast and HADA (cell wall) staining of 168 cultures at 24 h post-oxygen depletion. Cells were stained with HADA for the last doubling before oxygen was depleted and the dye was present during the duration of depletion. Orange arrowheads: phase-dark spherical cells that lack cell wall staining. Scale bar: 5 μm.

686 (B) 168 Δ*lytC* mutants remain rod-shaped following oxygen depletion. Left: OD_{600} of
687 168 Δ*lytC* exhibited somewhat slower lysis than the parent. Right: overlay of phase-
688 contrast and propidium iodide staining of 168 Δ*lytC* cells.
689 (C) Almost all 3610 cells grow once oxygen is restored following 24 h of oxygen
690 depletion, but only ~1% of 168 cells grow in similar circumstance. Cells from 3610
691 and 168 cultures after 24 h of oxygen depletion were spotted onto an LB pad and
692 imaged in time-lapse to determine which cells were capable of growing and
693 dividing. For 3610, the arrowhead points to a rare rod-shaped cell that did not
694 grow. For 168, the arrowhead points to a rare rod-shaped cell that grew. Scale bar:
695 10 μm. n = 536 and 604 rod-shaped cells for 3610 and 168, respectively. Images
696 shown are frames from Movies S3 and S4.

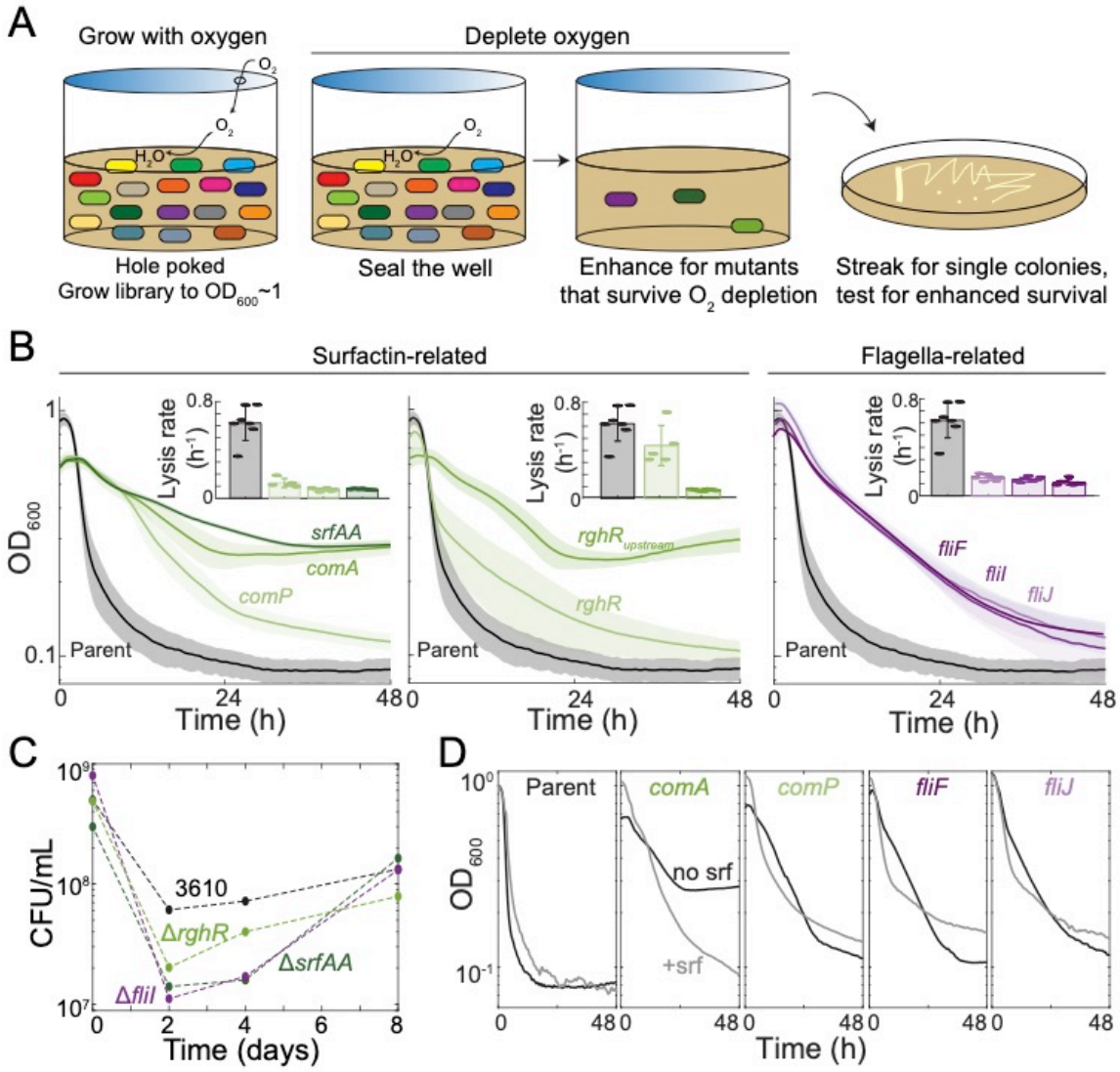

Figure S3: Characterization of hits from transposon screen. (Related to Figure 4)

(A) Schematic of transposon screen design. A transposon mutant library was grown to an OD_{600}~1, and then oxygen was depleted. We screened cells that were able to recover after oxygen depletion for oxygen depletion phenotypes.

(B) Transposon mutants have a reduced lysis rate. OD_{600} curves during oxygen depletion of cultures related to surfactin regulation (green) or flagella (purple). Lines represent the average and shading represents 1 SD, *n*=5. Inset: maximum lysis rates. Error bars represent 1 SD, *n*=5.

706 (C) Plating efficiency of clean deletions of *srfAA, fliI,* and *rghR* are lower than that of

707 3610 2 and 4 days following oxygen depletion.

708 (D) Addition of 48 μM surfactin increases the lysis rate of hits from transposon mutant

709 screen.

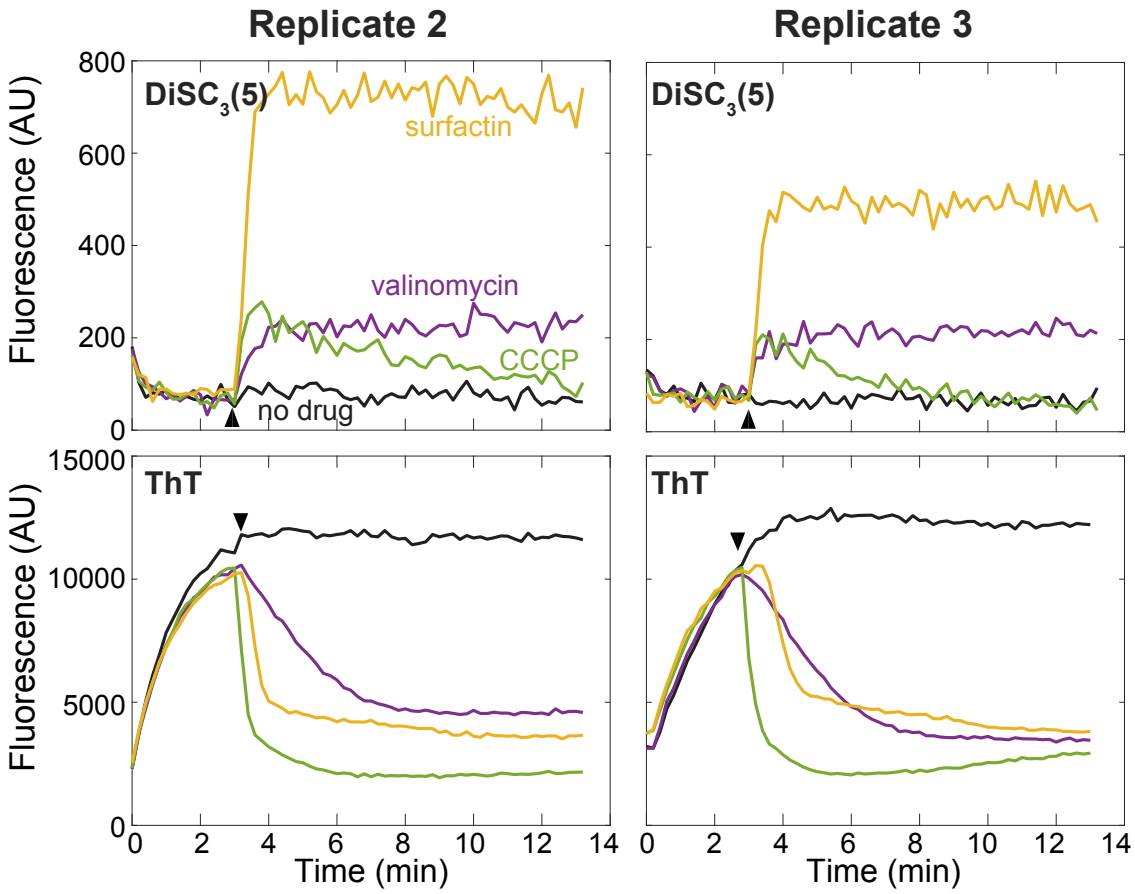

710

711 **Figure S4: Membrane potential assays of 168 cells. (Related to Figure 5)**

712 $DiSC_3(5)$ (top) and ThT (bottom) both show that surfactin (48 μM), valinomycin (50

713 μM) and CCCP (5 μM) (time of addition marked by the black arrow) cause

714 depolarization. Two experimental replicates are shown (replicate 1 is shown in Fig. 5).

715

716 **Supplemental Movie Legends**

717

718 **Supplemental Movie 1:** The majority of oxygen-depleted cells from strain 3610 grow once
719 oxygen is restored. Cells from a 24 h oxygen-depleted wild-type 3610 culture were spotted
720 onto an LB pad and imaged every 5 min at 37 °C. This experiment was done in tandem with
721 the 3610 Δ*lytC* cultures in Movie S2.

722

723 **Supplemental Movie 2:** A small subset of oxygen-depleted cells in the 3610 Δ*lytC* cultures
724 grow once oxygen is restored. Cells from a 24 h oxygen-depleted Δ*lytC* culture were spotted
725 on an LB pad and imaged every 5 min at 37 °C. This experiment was done in tandem with
726 the 3610 cultures in Movie S1.

727

728 **Supplemental Movie 3:** The majority of oxygen-depleted cells from strain 3610 grow once
729 oxygen is restored. This experiment was carried out as in Movie S1, and was done in
730 tandem with the 168 cultures in Movie S4.

731

732 **Supplemental Movie 4:** A very small subset of oxygen-depleted, rod-shaped cells from
733 strain 168 grow once oxygen is restored. Cells from a 24 h oxygen-depleted culture were
734 spotted on an LB pad and imaged every 5 min at 37 °C. This experiment was done in
735 tandem with the 3610 cultures in Movie S3.

736

737 **Supplemental Tables**

738 **Table S1: Information about hits from transposon screen.**

Gene hit	# independent hits	Gene function
srfAA	1	surfactin synthetase
comA	3	*comP/comA* quorum sensing response regulator
comP	4	*comP/comA* quorum sensing sensor histidine kinase
rghRA	1	transcriptional repressor
rghRA-upstream	1	transcriptional repressor
fliI	1	flagella chaperone
fliF	1	flagella chaperone
fliJ	1	flagella basal ring

739

740 **Table S2: List of strains used in this study.**

Strain name	Nickname	Genotype	Reference or source
HA10	3610	*trpC+, rapP+, sfp+, epsC+, swrA+, degQ+, pBS32*	Kearns lab
DK5073	3610 *ΔlytC*	3610, Δ*lytC*	This work
DK5075	3610 *ΔlytD*	3610, Δ*lytD*	This work
HA1	168	*trpC2*	Carol Gross lab
BKE35620	168 *ΔlytC*	168, Δ*lytC::MLS*	[14]
HA1417	168*sfp+*	168, *swrAfs, sfp⁰, amyE::Psfp-sfp cmR*	This work
HA1161	parent	3610, Δ*SPB*, Δ*PBSX*, Δ*pBS32*	Kearns lab
HA1235	N/A	3610, Δ*SPB*, Δ*PBSX*, Δ*pBS32*, *pMarA-kan*	This work
HA1414	N/A	168, *pMarA-kan*	This work
Back-crossed transposon mutagenesis strains			
HA1225	*comA*	3610, Δ*SPB*, Δ*PBSX*, Δ*pBS32*, *comA::pMarA-kan*	This work
HA1227	*comP*	3610, Δ*SPB*, Δ*PBSX*, Δ*pBS32*, *comP::pMarA-kan*	This work
HA1228	*fliJ*	3610, Δ*SPB*, Δ*PBSX*, Δ*pBS32*, *fliJ::pMarA-kan*	This work
HA1229	*fliI*	3610, Δ*SPB*, Δ*PBSX*, Δ*pBS32*, *fliI::pMarA-kan*	This work
HA1233	*fliF*	3610, Δ*SPB*, Δ*PBSX*, Δ*pBS32*, *fliF::pMarA-kan*	This work
HA1234	*srfAA*	3610, Δ*SPB*, Δ*PBSX*, Δ*pBS32*, *srfAA::pMarA-kan*	This work
HA1281	*yvaN*	3610, Δ*SPB*, Δ*PBSX*, Δ*pBS32*, *yvaN::pMarA-kan*	This work
HA1282	*yvaN-us (upstream)*	3610, Δ*SPB*, Δ*PBSX*, Δ*pBS32*, *yvaN-upstream::pMarA-kan*	This work
Clean deletions of transposon mutagenesis strains			
HA1369	Δ*srfAA*	3610, *srfAA*	This work
HA1374	Δ*fliI*	3610, *fliI*	This work
HA1377	Δ*rghRA*	3610, *rghRA*	This work

BKECG 168 strains used to create clean deletions in 3610			
BKE03480	N/A	168, *srfAA::MLS*	[14]
BKE16240	N/A	168, *fliI::MLS*	[14]
BKE33660	N/A	168, *rghRA::MLS*	[14]

741

742 **Table S3: Primers and plasmids used in this study.**

Primer number	Construct name	Sequence	Reference
1427	lytCUF SalI	AGGAGGTCGACGAATTAGTCTTGATGGAAAGCAGTAT	This work
1428	lytCUR EagI	CTCCTCGGCCGAAGCTGTTGGCACAAAAAGTATGAG	This work
1425	lytCDF EagI	AGGAGCGGCCGCATCAGATGCAAGTAAATTGAAGCA	This work
1426	lytCDR BamHI	ctcctggatcccatgatttgttttgtaatacttggcat	This work
1429	lytDUR EagI	AGGAGCGGCCGAAAAAACTTAGAAAGTTGCAAATAG GCT	This work
1430	lytDUF SalI	CTCCTGTCGACTTGATATGAAGAATAGACAGTTGGCA	This work
1431	lytDDR BamHI	AGGAGGGATCCAGTATTCCTTCAGAATCAACGGGGGA AT	This work
1432	lytDDF EagI	CTCCTCGGCCGTTAGTCTCTTTTTCATTCCTTCTCCTC TT	This work
695	IPCR1	GCTTGTAAATTCTATCATAATTG	This work
696	IPCR2	AGGGAATCATTTGAAGGTTGG	This work
Plasmids		**Genotype**	**Reference**
pDP299		*ΔlytC* ori^{TsBs} *mls amp*	This work
pDP300		*ΔlytD* ori^{TsBs} *mls amp*	This work
pMiniMAD		ori^{TsBs} *mls amp*	[59]
pDR244		ori^{Ts} *, cre constitutively expressed, amp/spc*	[14]

743

744 **References**

745

746 1. Boutilier, R.G. (2001). Mechanisms of cell survival in hypoxia and hypothermia. J Exp
747 Biol *204*, 3171-3181.
748 2. Hochachka, P.W. (1986). Defense strategies against hypoxia and hypothermia.
749 Science *231*, 234-241.
750 3. Sendoel, A., and Hengartner, M.O. (2014). Apoptotic cell death under hypoxia.
751 Physiology (Bethesda) *29*, 168-176.
752 4. Prescott, L.M., Harley, J.P., and Klein, D.A. (2005). Microbiology, 6th Edition,
753 (Dubuque, IA: McGraw-Hill Higher Education).
754 5. Wayne, L.G., and Hayes, L.G. (1996). An in vitro model for sequential study of
755 shiftdown of *Mycobacterium tuberculosis* through two stages of nonreplicating
756 persistence. Infect Immun *64*, 2062-2069.
757 6. Rao, S.P., Alonso, S., Rand, L., Dick, T., and Pethe, K. (2008). The protonmotive force
758 is required for maintaining ATP homeostasis and viability of hypoxic, nonreplicating
759 *Mycobacterium tuberculosis*. Proc Natl Acad Sci U S A *105*, 11945-11950.
760 7. Berney, M., Greening, C., Conrad, R., Jacobs, W.R., Jr., and Cook, G.M. (2014). An
761 obligately aerobic soil bacterium activates fermentative hydrogen production to
762 survive reductive stress during hypoxia. Proc Natl Acad Sci U S A *111*, 11479-11484.
763 8. O'Toole, R., Smeulders, M.J., Blokpoel, M.C., Kay, E.J., Lougheed, K., and Williams, H.D.
764 (2003). A two-component regulator of universal stress protein expression and
765 adaptation to oxygen starvation in *Mycobacterium smegmatis*. J Bacteriol *185*, 1543-
766 1554.

767 9. Nakano, M.M., Dailly, Y.P., Zuber, P., and Clark, D.P. (1997). Characterization of
768 anaerobic fermentative growth of *Bacillus subtilis*: identification of fermentation end
769 products and genes required for growth. J Bacteriol *179*, 6749-6755.
770 10. Pusey, P.L., and Wilson, C.L. (1984). Postharvest biological control of stone fruit
771 brown rot by *Bacillus subtilis*. Plant Disease *68*, 753-756.
772 11. Kumar, A.S., Lakshmanan, V., Caplan, J.L., Powell, D., Czymmek, K.J., Levia, D.F., and
773 Bais, H.P. (2012). Rhizobacteria *Bacillus subtilis* restricts foliar pathogen entry
774 through stomata. The Plant Journal *72*, 694-706.
775 12. Sierra, J., and Renault, P. (1998). Temporal Pattern of Oxygen Concentration in a
776 Hydromorphic Soil. Soil Science Society of America Journal *62*, 1398-1405.
777 13. Kaufman, W., and Bauer, K. (1958). Some studies of the mechanism of the" anaerobic
778 autolysis" of *Bacillus subtilis* J. Gen. Microbiol. *18*.
779 14. Koo, B.M., Kritikos, G., Farelli, J.D., Todor, H., Tong, K., Kimsey, H., Wapinski, I.,
780 Galardini, M., Cabal, A., Peters, J.M., et al. (2017). Construction and Analysis of Two
781 Genome-Scale Deletion Libraries for *Bacillus subtilis*. Cell Syst *4*, 291-305 e297.
782 15. Peters, J.M., Colavin, A., Shi, H., Czarny, T.L., Larson, M.H., Wong, S., Hawkins, J.S., Lu,
783 C.H.S., Koo, B.M., Marta, E., et al. (2016). A Comprehensive, CRISPR-based Functional
784 Analysis of Essential Genes in Bacteria. Cell *165*, 1493-1506.
785 16. Zhu, B., and Stulke, J. (2018). SubtiWiki in 2018: from genes and proteins to
786 functional network annotation of the model organism *Bacillus subtilis*. Nucleic Acids
787 Res *46*, D743-D748.

788 17. Zeigler, D.R., Pragai, Z., Rodriguez, S., Chevreux, B., Muffler, A., Albert, T., Bai, R.,
789 Wyss, M., and Perkins, J.B. (2008). The origins of 168, W23, and other *Bacillus*
790 *subtilis* legacy strains. J Bacteriol *190*, 6983-6995.
791 18. Julkowska, D., Obuchowski, M., Holland, I.B., and Seror, S.J. (2005). Comparative
792 analysis of the development of swarming communities of Bacillus subtilis 168 and a
793 natural wild type: critical effects of surfactin and the composition of the medium. J
794 Bacteriol *187*, 65-76.
795 19. Nakano, M.M., Corbell, N., Besson, J., and Zuber, P. (1992). Isolation and
796 characterization of sfp: a gene that functions in the production of the lipopeptide
797 biosurfactant, surfactin, in Bacillus subtilis. Mol Gen Genet *232*, 313-321.
798 20. Nakano, M.M., Marahiel, M.A., and Zuber, P. (1988). Identification of a genetic locus
799 required for biosynthesis of the lipopeptide antibiotic surfactin in *Bacillus subtilis*. J
800 Bacteriol *170*, 5662-5668.
801 21. Arima, K., Kakinuma, A., and Tamura, G. (1968). Surfactin, a crystalline peptidelipid
802 surfactant produced by *Bacillus subtilis*: isolation, characterization and its inhibition
803 of fibrin clot formation. Biochem Biophys Res Commun *31*, 488-494.
804 22. Płaza, G.A., Turek, A., Król, E., and Szczygłowska, R. (2013). Antifungal and
805 antibacterial properties of surfactin isolated from *Bacillus subtilis* growing on
806 molasses. African Journal of Microbiology Research *7*, 3165-3170.
807 23. Korenblum, E., de Araujo, L.V., Guimaraes, C.R., de Souza, L.M., Sassaki, G., Abreu, F.,
808 Nitschke, M., Lins, U., Freire, D.M., Barreto-Bergter, E., et al. (2012). Purification and
809 characterization of a surfactin-like molecule produced by *Bacillus sp. H2O-1* and its
810 antagonistic effect against sulfate reducing bacteria. BMC Microbiol *12*, 252.

811 24. Rosenberg, G., Steinberg, N., Oppenheimer-Shaanan, Y., Olender, T., Doron, S., Ben-
812 Ari, J., Sirota-Madi, A., Bloom-Ackermann, Z., and Kolodkin-Gal, I. (2016). Not so
813 simple, not so subtle: the interspecies competition between *Bacillus simplex* and
814 *Bacillus subtilis* and its impact on the evolution of biofilms. NPJ Biofilms
815 Microbiomes *2*, 15027.
816 25. Snook, M.E., Mitchell, T., Hinton, D.M., and Bacon, C.W. (2009). Isolation and
817 characterization of leu7-surfactin from the endophytic bacterium *Bacillus*
818 *mojavensis* RRC 101, a biocontrol agent for *Fusarium verticillioides*. J Agric Food
819 Chem *57*, 4287-4292.
820 26. Zhi, Y., Wu, Q., Du, H., and Xu, Y. (2016). Biocontrol of geosmin-producing
821 Streptomyces spp. by two *Bacillus* strains from Chinese liquor. Int J Food Microbiol
822 *231*, 1-9.
823 27. Olmeda, B., Villen, L., Cruz, A., Orellana, G., and Perez-Gil, J. (2010). Pulmonary
824 surfactant layers accelerate O(2) diffusion through the air-water interface. Biochim
825 Biophys Acta *1798*, 1281-1284.
826 28. Cabeen, M.T., and Jacobs-Wagner, C. (2005). Bacterial cell shape. Nat Rev Microbiol
827 *3*, 601-610.
828 29. Lazarevic, V., Margot, P., Soldo, B., and Karamata, D. (1992). Sequencing and analysis
829 of the *Bacillus subtilis lytRABC* divergon: a regulatory unit encompassing the
830 structural genes of the N-acetylmuramoyl-L-alanine amidase and its modifier. J Gen
831 Microbiol *138*, 1949-1961.

832 30. Margot, P., Mauel, C., and Karamata, D. (1994). The gene of the N-
833 acetylglucosaminidase, a *Bacillus subtilis* 168 cell wall hydrolase not involved in
834 vegetative cell autolysis. Mol Microbiol *12*, 535-545.
835 31. Koch, A.L. (2001). Autolysis control hypotheses for tolerance to wall antibiotics.
836 Antimicrob Agents Chemother *45*, 2671-2675.
837 32. Sheppard, J.D., Jumarie, C., Cooper, D.G., and Laprade, R. (1991). Ionic channels
838 induced by surfactin in planar lipid bilayer membranes. Biochim Biophys Acta *1064*,
839 13-23.
840 33. Laidig, K.E., Gainer, J.L., and Daggett, V. (1998). Altering Diffusivity in Biological
841 Solutions through Modification of Solution Structure and Dynamics. J Am Chem Soc
842 *120*, 9394-9395.
843 34. Hotez, L., Dailey, J.W., Geelhoed, G.W., and Gainer, J.L. (1977). The role of oxygen
844 diffusivity in biochemical reactions. Experientia *33*, 1424-1425.
845 35. Cosmina, P., Rodriguez, F., de Ferra, F., Grandi, G., Perego, M., Venema, G., and van
846 Sinderen, D. (1993). Sequence and analysis of the genetic locus responsible for
847 surfactin synthesis in *Bacillus subtilis*. Mol Microbiol *8*, 821-831.
848 36. Nakano, M.M., Xia, L.A., and Zuber, P. (1991). Transcription initiation region of the
849 *srfA* operon, which is controlled by the *comP-comA* signal transduction system in
850 *Bacillus subtilis*. J Bacteriol *173*, 5487-5493.
851 37. Hayashi, K., Kensuke, T., Kobayashi, K., Ogasawara, N., and Ogura, M. (2006). *Bacillus*
852 *subtilis* RghR (YvaN) represses *rapG* and *rapH*, which encode inhibitors of
853 expression of the *srfA* operon. Mol Microbiol *59*, 1714-1729.

854 38. Mukherjee, S., and Kearns, D.B. (2014). The structure and regulation of flagella in
855 *Bacillus subtilis*. Annu Rev Genet *48*, 319-340.
856 39. Ueno, T., Oosawa, K., and Aizawa, S. (1992). M ring, S ring and proximal rod of the
857 flagellar basal body of *Salmonella typhimurium* are composed of subunits of a single
858 protein, FliF. J Mol Biol *227*, 672-677.
859 40. Evans, L.D., Stafford, G.P., Ahmed, S., Fraser, G.M., and Hughes, C. (2006). An escort
860 mechanism for cycling of export chaperones during flagellum assembly. Proc Natl
861 Acad Sci U S A *103*, 17474-17479.
862 41. Minamino, T., Chu, R., Yamaguchi, S., and Macnab, R.M. (2000). Role of FliJ in flagellar
863 protein export in *Salmonella*. J Bacteriol *182*, 4207-4215.
864 42. Farha, M.A., Verschoor, C.P., Bowdish, D., and Brown, E.D. (2013). Collapsing the
865 proton motive force to identify synergistic combinations against *Staphylococcus*
866 *aureus*. Chem Biol *20*, 1168-1178.
867 43. Prindle, A., Liu, J., Asally, M., Ly, S., Garcia-Ojalvo, J., and Suel, G.M. (2015). Ion
868 channels enable electrical communication in bacterial communities. Nature *527*, 59-
869 63.
870 44. Varma, S., Sabo, D., and Rempe, S.B. (2008). K+/Na+ selectivity in K channels and
871 valinomycin: over-coordination versus cavity-size constraints. J Mol Biol *376*, 13-22.
872 45. Strahl, H., Burmann, F., and Hamoen, L.W. (2014). The actin homologue MreB
873 organizes the bacterial cell membrane. Nat Commun *5*, 3442.
874 46. Branda, S.S., Gonzalez-Pastor, J.E., Ben-Yehuda, S., Losick, R., and Kolter, R. (2001).
875 Fruiting body formation by *Bacillus subtilis*. Proc Natl Acad Sci U S A *98*, 11621-
876 11626.

877 47. Pham, J.V., Yilma, M.A., Feliz, A., Majid, M.T., Maffetone, N., Walker, J.R., Kim, E., Cho,
878 H.J., Reynolds, J.M., Song, M.C., et al. (2019). A Review of the Microbial Production of
879 Bioactive Natural Products and Biologics. Front Microbiol *10*, 1404.
880 48. Hu, J., Lei, P., Mohsin, A., Liu, X., Huang, M., Li, L., Hu, J., Hang, H., Zhuang, Y., and Guo,
881 M. (2017). Mixomics analysis of Bacillus subtilis: effect of oxygen availability on
882 riboflavin production. Microb Cell Fact *16*, 150.
883 49. Garcia-Ochoa, F., and Gomez, E. (2009). Bioreactor scale-up and oxygen transfer rate
884 in microbial processes: an overview. Biotechnol Adv *27*, 153-176.
885 50. Baeshen, N.A., Baeshen, M.N., Sheikh, A., Bora, R.S., Ahmed, M.M., Ramadan, H.A.,
886 Saini, K.S., and Redwan, E.M. (2014). Cell factories for insulin production. Microb
887 Cell Fact *13*, 141.
888 51. Arjes, H.A., Kriel, A., Sorto, N.A., Shaw, J.T., Wang, J.D., and Levin, P.A. (2014). Failsafe
889 mechanisms couple division and DNA replication in bacteria. Curr Biol *24*, 2149-
890 2155.
891 52. Rojas, E.R., Huang, K.C., and Theriot, J.A. (2017). Homeostatic Cell Growth Is
892 Accomplished Mechanically through Membrane Tension Inhibition of Cell-Wall
893 Synthesis. Cell Syst *5*, 578-590 e576.
894 53. Blackman, S.A., Smith, T.J., and Foster, S.J. (1998). The role of autolysins during
895 vegetative growth of *Bacillus subtilis* 168. Microbiology *144 (Pt 1)*, 73-82.
896 54. Calamita, H.G., Ehringer, W.D., Koch, A.L., and Doyle, R.J. (2001). Evidence that the
897 cell wall of Bacillus subtilis is protonated during respiration. Proc Natl Acad Sci U S
898 A *98*, 15260-15263.

899 55. Mueller, E.A., Egan, A.J., Breukink, E., Vollmer, W., and Levin, P.A. (2019). Plasticity of
900 *Escherichia coli* cell wall metabolism promotes fitness and antibiotic resistance
901 across environmental conditions. Elife *8*.
902 56. Peters, K., Kannan, S., Rao, V.A., Biboy, J., Vollmer, D., Erickson, S.W., Lewis, R.J.,
903 Young, K.D., and Vollmer, W. (2016). The Redundancy of Peptidoglycan
904 Carboxypeptidases Ensures Robust Cell Shape Maintenance in *Escherichia coli*. MBio
905 *7*.
906 57. Stratford, J.P., Edwards, C.L.A., Ghanshyam, M.J., Malyshev, D., Delise, M.A., Hayashi,
907 Y., and Asally, M. (2019). Electrically induced bacterial membrane-potential
908 dynamics correspond to cellular proliferation capacity. Proc Natl Acad Sci U S A *116*,
909 9552-9557.
910 58. Yasbin, R.E., and Young, F.E. (1974). Transduction in *Bacillus subtilis* by
911 bacteriophage SPP1. J Virol *14*, 1343-1348.
912 59. Patrick, J.E., and Kearns, D.B. (2008). MinJ (YvjD) is a topological determinant of cell
913 division in *Bacillus subtilis*. Mol Microbiol *70*, 1166-1179.
914 60. Arnaud, M., Chastanet, A., and Debarbouille, M. (2004). New vector for efficient
915 allelic replacement in naturally nontransformable, low-GC-content, gram-positive
916 bacteria. Appl Environ Microbiol *70*, 6887-6891.
917 61. DeRosa, C.A., Samonina-Kosicka, J., Fan, Z., Hendargo, H.C., Weitzel, D.H., Palmer,
918 G.M., and Fraser, C.L. (2015). Oxygen Sensing Difluoroboron Dinaphthoylmethane
919 Polylactide. Macromolecules *48*, 2967-2977.
920 62. DeRosa, C.A., Seaman, S.A., Mathew, A.S., Gorick, C.M., Fan, Z., Demas, J.N., Peirce,
921 S.M., and Fraser, C.L. (2016). Oxygen Sensing Difluoroboron beta-Diketonate

922 Polylactide Materials with Tunable Dynamic Ranges for Wound Imaging. ACS Sens *1*,
923 1366-1373.
924 63. Shi, H., Colavin, A., Lee, T.K., and Huang, K.C. (2017). Strain Library Imaging Protocol:
925 high-throughput, automated single-cell microscopy for large bacterial collections
926 arrayed on multiwell plates. Nature Protocols.
927 64. Kuru, E., Hughes, H.V., Brown, P.J., Hall, E., Tekkam, S., Cava, F., de Pedro, M.A., Brun,
928 Y.V., and VanNieuwenhze, M.S. (2012). In Situ probing of newly synthesized
929 peptidoglycan in live bacteria with fluorescent D-amino acids. Angew Chem Int Ed
930 Engl *51*, 12519-12523.

931